provide the requisite adjustment in redox potential.

Summary and Conclusions. The manganese(III) analogues of the iron(III) hemerythrin model complexes, $[Mn_2O(O_2CR)_2(HB(pz)_3)_2]$, have been synthesized and characterized in this study. The major differences between the two classes of molecules derive from removal of a d-electron on each metal center from the d_{z^2} orbital directed along the metal-μ-oxo vectors in going from the d^5-d^5, Fe_2(III,III) to the d^4-d^4, Mn_2(III,III) system. The consequences of this change in electronic structure are manifest in differences in the metal-ligand bond lengths trans to the bridging oxygen atom and, more importantly, a markedly diminished antiferromagnetic spin exchange interaction in the dimanganese complex. The greater paramagnetism and faster spin relaxation of the latter leads to relatively sharp, contact-shifted ligand proton resonances in the NMR spectrum that will be valuable in identifying dimanganese centers of this kind in biology. Moreover, these results suggest that substitution of Mn(III) for Fe(III), if it could be experimentally achieved in proteins containing the $\{Fe_2O\}^{4+}$ core, would be a powerful way to probe the nature of these centers in iron-oxo proteins such as ribonucleotide reductase.

Acknowledgment. This work was supported by research grants from the National Institutes of Health General Medical Institute GM-32134 (to S.J.L.) and the National Science Foundation CHE82-17920 (to G.C.D.). Additional support is acknowledged by G.C.D. for an Alfred P. Sloan Foundation Fellowship, by J.E.S. for a faculty research fellowship from Rider College, by J.S. for an NIH Research Career Development Award AM-01222, by W.H. Armstrong from NCI Training Grant CA-09112, and by G.C.D. and V.P. for a NATO travel grant (236/83). We thank the Biomedical Research Support Shared Instrumentation grant program, Division of Research Resources, for funds to purchase the X-ray diffraction equipment (at MIT), NIH Grant RR-02243, Dr. J. C. Dewan for obtaining the low-temperature X-ray data, P. N. Turowski for obtaining spectroscopic data, and S. Artandi for assistance with synthesis. Magnetic data were taken at the Francis Bitter National Magnet Laboratory which is supported by the National Science Foundation.

Note Added in Proof. Resonance R and mass spectrometric studies have recently shown this species to be $[(HB(pz)_3)Mn(O)_2(O_2CCH_3)Mn(HB(pz)_3)]$ (Sheats, J. E.; Unni Nair, B. C.; Petrouleas, V.; Artandi, S.; Dismukes, G. C., to be submitted for publication).

Supplementary Material Available: Tables of thermal and hydrogen atom positional parameters for both $1{\cdot}4CH_3CN$ and $1{\cdot}CH_3CN$ and temperature dependent magnetic susceptibility data for the two compounds as separately measured at MIT and in Athens (6 pages); tables reporting observed and calculated structure factors for $1{\cdot}4CH_3CN$ and $1{\cdot}CH_3CN$ (24 pages). Ordering information is given on any current masthead page.

Relative Metal–Hydrogen, –Oxygen, –Nitrogen, and –Carbon Bond Strengths for Organoruthenium and Organoplatinum Compounds; Equilibrium Studies of $Cp^*(PMe_3)_2RuX$ and (DPPE)MePtX Systems

Henry E. Bryndza,*[1] Lawrence K. Fong,[2] Rocco A. Paciello,[2] Wilson Tam,[1] and John E. Bercaw*[2]

Contribution No. 4056 from the Central Research and Development Department of the E. I. DuPont de Nemours & Co., Inc., Experimental Station, Wilmington, Delaware 19898, and Contribution No. 7397 from the California Institute of Technology, Pasadena, California 91125.
Received April 18, 1986

Abstract: A series of ruthenium, $Cp^*(PMe_3)_2RuX$ ($Cp^* = \eta^5$-C_5Me_5), and platinum, (DPPE)MePtX (DPPE = $Ph_2PCH_2CH_2PPh_2$), compounds have been prepared. The equilibria L_nM–X + H–Y $\rightleftharpoons$ L_nM–Y + H–X (L_nM = (DPPE)MePt or $Cp^*(PMe_3)_2Ru$; X, Y = hydride, alkoxide, hydroxide, amide, alkyl, alkynyl, hydrosulfide, cyanide) have been examined. A lower limit of the Ru–N bond strength has been estimated by analysis of the kinetics of the thermal decomposition of $Cp^*(PMe_3)_2RuNPh_2$. The equilibrium constants allow for the determination of relative M–X, M–Y bond dissociation energies (BDEs) for each series of compounds. A linear correlation of L_nM–X to H–X BDEs is found for the two dissimilar metal centers. The generality to other systems and predictive value of this correlation are discussed.

Despite the widespread use of organometallic catalysts to effect homogeneous organic transformations, little is known about the thermochemistry of individual steps comprising catalytic cycles. Recent advances have led to values for some metal–hydrogen and metal–carbon bond strengths,[3] but the factors governing the reactivity of transition metal–heteroatom bonds (M–X: X = OH, OR, NR_2, PR_2, SiR_3, and SH) have been left relatively unexplored.

Early transition metal–oxygen and –nitrogen bonds are quite robust, presumably due to ligand-to-metal π-donation of an oxygen or nitrogen lone electron pair to an empty orbital of the electrophilic metal center.[4] In contrast, there has been a common perception that late transition metal–nitrogen and –oxygen linkages are intrinsically weak due to the mismatch of hard ligand base with soft metal acid,[5] thus explaining the relative scarcity of such complexes in the literature. Only recently has the reaction

(1) E. I. DuPont de Nemours & Company, Inc. Central Research and Development Department.
(2) California Institute of Technology.
(3) For leading references see: (a) Connor, J. A. *Top. Curr. Chem.* **1977**, *71*, 71. (b) Halpern, J. *Acc. Chem. Res.* **1982**, *15*, 238. (c) Pearson, R. G. *Chem. Rev.* **1985**, *85*, 41. (d) Halpern, J. *Inorg. Chim. Acta* **1985**, *100*, 41. (e) Martinho Simoes, J. A.; Beauchamp, J. L. *Chem. Rev., in press.*
(4) Connor, J. A. *Top. Curr. Chem.* **1977**, *71*, 71.
(5) (a) Pearson, R. G. *J. Am. Chem. Soc.* **1963**, *85*, 3533. (b) Pearson, R. G. *J. Chem. Educ.* **1968**, *45*, 643.

0002-7863/87/1509-1444$01.50/0

chemistry of late transition metal alkoxides and amides been examined.[6]

Recent examples of the types of reaction chemistry available to late metal–oxygen and –nitrogen bonds include CO[7] and olefin[8] insertions, β-hydride elimination,[9] and "σ bond metathesis" reactions;[10] the last provide a means of determining relative metal–X σ bond strengths for a series of complexes. In this paper we report L_nM–X bond strengths obtained from measurements of the equilibrium constants for a series of reactions involving Cp*(PMe$_3$)$_2$RuX (Cp* = η^5-C_5Me_5) and (DPPE)MePtX (DPPE = $Ph_2PCH_2CH_2PPh_2$) complexes.

Results

1. Synthesis. Our initial efforts were directed toward the synthesis of well-defined, monomeric hydroxide, amide, and alkoxide derivatives of group VIII metals. Syntheses of some of the (DPPE)MePtX and Cp*(PMe$_3$)$_2$RuX complexes utilized in our studies have been published previously.[11] Syntheses of the new Cp*(PMe$_3$)$_2$RuX and (DPPE)MePtX derivatives are described below.

Cp*(PMe$_3$)$_2$RuOH (**1**) is prepared by treating a diethyl ether solution of Cp*(PMe$_3$)$_2$RuR (**2**: R = CH_3; **3**: R = CH_2SiMe_3) with 1.05 equiv of triflic acid, followed by reaction of the resultant cation with an aqueous THF solution of KOH (eq 1).[12] Extended reflux of Cp*(PMe$_3$)$_2$RuCl with KOH in THF/H_2O fails to yield the hydroxide complex **1**. The hydroxide compound, Cp*(PMe$_3$)$_2$RuOH (**1**), is best isolated after solvent removal and subsequent freeze–drying in benzene to give a material suitable for recrystallization. Cp*(PMe$_3$)$_2$RuOH crystallizes from an-

$$\underset{\mathbf{2}}{Cp^*(PMe_3)_2RuCH_3} \xrightarrow[Et_2O]{HSO_3CF_3} [Cp^*(PMe_3)_2Ru(CH_3)H]^+SO_3CF_3^- \xrightarrow[Et_2O]{-CH_4} [Cp^*(PMe_3)_2Ru(Et_2O)]^+SO_3CF_3^- \xrightarrow[THF]{KOH,H_2O} \underset{\mathbf{1}}{Cp^*(PMe_3)_2RuOH} + KSO_3CF_3 \quad (1)$$

hydrous petroleum ether solutions as stable orange-red crystals, which decompose on exposure to air. The anhydrous complex is monomeric in solution (M_r = 389; ebulliometry in C_6H_6), and a weak O–H stretch is observed at 3687 cm^{-1} in CH_2Cl_2 solution.[13] The NMR spectrum (benzene-d_6) for **1** exhibits a triplet at −5.57 ppm ($^3J_{P-H}$ = 3.66 Hz), assigned to the hydroxide proton. Compound **1** is less pentane soluble when even small amounts of water of hydration are present, and it can be readily isolated as a yellow crystalline solid from benzene/pentane mixtures in this hydrated form.[14]

Treatment of **1** with CO or ethylene (THF solution, 25 °C) leads to multiple products in either case. Traces of hydride were observed upon heating (35 °C) **1** with ethylene, while Cp*(PMe$_3$)Ru(CO)H, Cp*(PMe$_3$)$_2$RuH, and Cp*(PMe$_3$)$_2$RuCO$_2$H were observed on carbonylation.

The cationic Ru^{IV} hydrido methyl complex intermediate in the synthesis of **1** has been isolated as the tetrafluoroborate salt (**4**) (eq 2). Cation **4** precipitates from diethyl ether as it forms and

$$\underset{\mathbf{2}}{Cp^*(PMe_3)_2RuCH_3} + HBF_4 \xrightarrow{Et_2O} \underset{\mathbf{4}}{[Cp^*(PMe_3)_2Ru(CH_3)H]^+BF_4^-} \quad (2)$$

can be isolated in high yield as a relatively insoluble off-white powder. ^{1}H nuclear magnetic resonance (NMR) spectra obtained in acetone-d_6 (in which the compound decomposes in 1–2 h) show a triplet for the methyl group at 0.13 ppm ($^3J_{P-H}$ = 9.5 Hz) and an upfield triplet for the hydride at −10.0 ppm ($^2J_{P-H}$ = 41.8 Hz). The compound can be stored indefinitely under an inert atmosphere at −20 °C in the solid state, but it discolors slowly at room temperature.

All attempts to isolate the corresponding ruthenium methoxide complex, Cp*(PMe$_3$)$_2$RuOMe, by treating the cation with NaOMe under a wide variety of conditions (eq 3) have resulted

$$[Cp^*(PMe_3)_2Ru(Et_2O)]^+SO_3CF_3^- + NaOMe \rightarrow Cp^*(PMe_3)_2RuH \quad (3)$$

instead in isolation of Cp*(PMe$_3$)$_2$RuH from the product mixture. Refluxing Cp*(PMe$_3$)$_2$RuCl and sodium methoxide in methanol yields various ratios of Cp*(PMe$_3$)$_2$RuH and Cp*(PMe$_3$)$_2$RuCO$_2$CH$_3$ as the sole organometallic products. Treatment of hydroxide **1** with methanol in THF-d_8 at 0 °C leads to an unisolable intermediate species, which may be the methoxide, that ultimately gives Cp*(PMe$_3$)$_2$RuH.

The diphenylamide compound, Cp*(PMe$_3$)$_2$RuNPh$_2$ (**5**), is prepared by metathesis of Cp*(PMe$_3$)$_2$RuCl with LiNPh$_2$ in THF at room temperature (eq 4). Treatment of **5** with carbon monoxide

$$Cp^*(PMe_3)_2RuCl + LiNPh_2 \rightarrow \underset{\mathbf{5}}{Cp^*(PMe_3)_2RuNPh_2} \quad (4)$$

(6) (a) Cotton, F. A.; Wilkinson, G. *Advanced Inorganic Chemistry*, 4th ed.; Wiley: New York, 1980. (b) Mehrotra, R. C. *Adv. Inorg. Chem. Radiochem.* **1983**, *26*, 269. (c) Michelin, R. A.; Napoli, M.; Ros, R. *J. Organomet. Chem.* **1979**, *175*, 239. (d) Rees, W. M.; Atwood, J. D. *Organometallics* **1985**, *4*, 402. (e) Abel, E. W.; Farrow, G.; Towle, I. D. H. *J. Chem. Soc., Dalton Trans.* **1979**, 71. (f) Komiya, S.; Tane-ichi, S.; Yamamoto, A.; Yamamoto, T. *Bull. Chem. Soc. Jpn.* **1980**, *53*, 673. (g) Arnold, D. P.; Bennett, M. A. *J. Organomet. Chem.* **1980**, *199*, 119. (h) Yoshida, T.; Okano, T.; Otsuka, S. *J. Chem. Soc., Dalton Trans.* **1976**, 993. (i) Bennett, M. A.; Yoshida, T. *J. Am. Chem. Soc.* **1978**, *100*, 1750. (j) Bryndza, H. E.; Calabrese, J. C.; Wreford, S. S. *Organometallics* **1984**, *3*, 1603. (k) Bryndza, H. E.; Kretchmar, S. A.; Tulip, T. H. *J. Chem. Soc., Chem. Commun.* **1985**, 977. (l) Newman, L. J.; Bergman, R. G. *J. Am. Chem. Soc.* **1985**, *107*, 5314. (m) Coulson, D. R. *J. Am. Chem. Soc.* **1976**, *98*, 3111. (n) Bennett, M. A.; Robertson, G. B.; Whimp, P. O.; Yoshida, T. *J. Am. Chem. Soc.* **1973**, *95*, 3028. (o) Monaghan, P. K.; Puddephatt, R. J. *Organometallics* **1984**, *3*, 444. (p) Arnold, D. P.; Bennett, M. A. *Inorg. Chem.* **1984**, *23*, 2110. (q) Flynn, B. R.; Vaska, L. *J. Am. Chem. Soc.* **1973**, *95*, 5081. (r) Chaudret, B. N.; Cole-Hamilton, D. J.; Nohr, R. S.; Wilkinson, G. *J. Chem. Soc., Dalton Trans.* **1977**, 1546. (s) Fryzuk, M. D.; MacNeil, P. A. *Organometallics* **1983**, *2*, 355. (t) Fryzuk, M. D.; MacNeil, P. A. *Organometallics* **1983**, *2*, 682. (u) Fryzuk, M. D.; MacNeil, P. A.; Rettig, S. J.; Secco, A. S.; Trotter, J. *Organometallics* **1982**, *1*, 918. (v) Lappert, M. F.; Power, P. P.; Sanger, A. R.; Srivastava, R. C. *Metal and Metalloid Amides*; Ellis Horwood, 1980. (w) Beck, W.; Bauder, M. *Chem. Ber.* **1970**, *103*, 58. (x) Bryndza, H. E. *Organometallics* **1985**, *4*, 1686. (y) Bryndza, H. E. *Organometallics* **1985**, *4*, 406. (z) Bryndza, H. E.; Fultz, W. C.; Tam, W. *Organometallics* **1985**, *4*, 939.

(7) (a) Bryndza, H. E. *Organometallics* **1985**, *4*, 1686. (b) Bryndza, H. E.; Kretchmar, S. A.; Tulip, T. H. *J. Chem. Soc., Chem. Commun.* **1985**, 977. (c) Michelin, R. A.; Napoli, M.; Ros, R. *J. Organomet. Chem.* **1979**, *175*, 239. (d) Deeming, A. J.; Shaw, B. L. *J. Chem. Soc. A* **1969**, 443. (e) Bennett, M. A.; Yoshida, T. *J. Am. Chem. Soc.* **1978**, *100*, 1750. (f) Appleton, T. G.; Bennett, M. A. *J. Organomet. Chem.* **1973**, *55*, C88.

(8) (a) Bryndza, H. E.; Calabrese, J. C.; Wreford, S. S. *Organometallics* **1984**, *3*, 1603. (b) Bryndza, H. E. *Organometallics* **1985**, *4*, 406.

(9) (a) Bryndza, H. E.; Calabrese, J. C.; Marsi, M.; Roe, D. C.; Tam, W.; Bercaw, J. E. *J. Am. Chem. Soc.* **1986**, *108*, 4805. (b) Bennett, M. A.; Arnold, D. P. *J. Organomet. Chem.* **1980**, *199*, C17. (c) Arnold, D. P.; Bennett, M. A. *Inorg. Chem.* **1984**, *23*, 2110. (d) Yoshida, T.; Okano, T.; Otsuka, S. *J. Chem. Soc., Dalton Trans.* **1976**, 993. (e) Monaghan, P. K.; Puddephatt, R. J. *Organometallics* **1984**, *3*, 444. (f) Michelin, R. A.; Napoli, M.; Ros, R. *J. Organomet. Chem.* **1979**, *175*, 239. (g) Bernard, K. A.; Rees, W. M.; Atwood, J. D. *Organometallics* **1986**, *5*, 390.

(10) (a) Bryndza, H. E.; Fultz, W. C.; Tam, W. *Organometallics* **1985**, *4*, 939. (b) Appleton, T. G.; Bennett, M. A. *Inorg. Chem.* **1978**, *17*, 738.

(11) (a) Bryndza, H. E.; Calabrese, J. C.; Marsi, M.; Roe, D. C.; Tam, W.; Bercaw, J. E. *J. Am. Chem. Soc.* **1986**, *108*, 4805. (b) Appleton, T. G.; Bennett, M. A. *Inorg. Chem.* **1978**, *17*, 738. (c) Tilley, T. D.; Grubbs, R. H.; Bercaw, J. E. *Organometallics* **1984**, *3*, 274.

(12) Treatment of [Cp*(PMe$_3$)$_2$Ru·Et$_2$O]$^+$SO$_3$CF$_3^-$ with KOH in the absence of H_2O results in the formation of (η^4-$C_5Me_4CH_2$)Ru(PMe$_3$)$_3$; L. K. Fong and J. E. Bercaw, unpublished results.

(13) Weak OH absorbances are characteristic of late metal hydroxides, see, for example: (a) Michelin, R. A.; Napoli, M.; Ros, R. *J. Organomet. Chem.* **1979**, *175*, 239. (b) Yoshida, T.; Okano, T.; Otsuka, S. *J. Chem. Soc., Dalton Trans.* **1976**, 993.

(14) A cautionary note: the following observations have been made during the synthesis of Cp*(PMe$_3$)$_2$RuOH: (i) treatment of Cp*(PMe$_3$)$_2$RuOH with base (such as occurs during aqueous extraction of the Cp*(PMe$_3$)$_2$RuOH/KOH mixture) leads to formation of the dimer, (Cp*(PMe$_3$)$_2$Ru)$_2$O, and (ii) the following equilibrium has been observed in diethyl ether: 3Cp*(PMe$_3$)$_2$RuOH ⇌ (Cp*(PMe$_3$)$_2$Ru)O + Cp*(PMe$_3$)$_2$RuOH·H_2O. The dimer can be cleaved, however, to give Cp*(PMe$_3$)$_2$RuOH·H_2O with use of excess H_2O.

Table I. ^1H and $^{31}P[^1H]$ NMR Data for $Cp^*(PMe_3)_2RuX$ Complexes

	^1H[a]						^{31}P[e]	
compound	C_5Me_5[b]	T_1[c]	PMe_3[d]	T_1[c]	other assignments[j]			T_1[c]
$Cp^*(PMe_3)_2RuOH$	1.69 (1.34)	3.8	1.34 (7.81)	2.78	RuOH	−5.57 (t, $^3J_{P-H}$ = 3.66)	3.10	10.94
$[Cp^*(PMe_3)_2Ru(Me)H]BF_4$[f]	1.85 (g)	h	1.51 (10.21)	h	Ru—CH_3	−0.13 (t, $^3J_{P-H}$ = 9.52)	10.49	h
					Ru—H	−10.00 (t, $^2J_{P-H}$ = 41.75)		
$Cp^*(PMe_3)_2RuNPh_2$	1.66 (1.59)	1.43	1.29 (7.77)	1.14	$RuNPH_2$	7.1 (m), 6.9 (m), 6.6 (m), 6.3 (m)	0.51	5.43
$Cp^*(PMe_3)_2RuSH$	1.69 (1.44)	4.67	1.35 (8.10)	3.02	RuSH	−4.54 (t, $^3J_{P-H}$ = 8.42, T_1 = 15.13)	5.85	14.30
$Cp^*(PMe_3)_2RuCN$	1.82 (1.47)	4.27	1.43 (7.83)	2.64			7.33	12.30
$Cp^*(PMe_3)_2RuCH_2(CO)CH_3$	1.69 (1.41)	5.90	1.54 (7.83)	3.20	$RuCH_2Me$	1.38 (t, $^3J_{P-H}$ = 0.49); T_1 = 3.2	6.30	11.30
					$RuCH_2CH_3$	1.80 (s); T_1 = 4.0		
$Cp^*(PMe_3)_2Ru—C\equiv C—Ph$	1.82 (1.19)	3.01	1.42 (8.74)	1.67	Ru—C≡C—Ph	7.02 (m), 6.96 (m), 6.8 (m)	8.74	8.1
$Cp^*(PMe_3)_2RuNHPh$	1.69 (1.52)	2.34	1.37 (7.95)	1.52	Ru—N*H*Ph	g	5.51	7.2
					Ru—NH*Ph*	6.51 (m), 6.05 (m), 5.6 (m)		
$Cp^*(PMe_3)_2Ru—Mo(CO)_3Cp$	1.35 (g)	3.00	1.09 (7.92)	2.52	C_5H_5	5.32 (s); T_1 = 21.08	0.29	10.00
$Cp^*(PMe_3)_2Ru—W(CO)_3Cp$	1.38 (1.30)	2.81	1.11 (8.05)	1.80	C_5H_5	5.22 (s); T_1 = 22.07	1.32	11.95
$Cp^*(PMe_3)(PHPh_2)RuSH$	1.60 (1.80)	h	1.08 (8.40)[i]	h	P*H*Ph_3	6.95 (d, $^1J_{P-H}$ = 345)		
					PH*Ph*$_2$	g		
					Ru—SH	−3.50 (dd, $^3J_{P-H}$ = 7.5, 9.6)	41.36 ($^2J_{P-P}$ = 46.4)	h
							3.16	h
$Cp^*(PMe_3)Ru(\eta^2\text{-}PMe_3CH_2)$	1.92 (1.59)	h	1.15 (d, 7.21)	h	$P(CH_3)_2$	1.29 (d, 9.76)	−2.3 (d, $^2J_{P-P}$ = 37)	h
						1.05 (d, 9.52)	39.5 (d, $^2J_{P-P}$ = 37)	
					PCH_2	−0.20 (ddd, $^2J_{P-H}$ = 13.0, $^4J_{P-H}$ = 1.35, $^2J_{H-H}$ = 7.60)		
						0.53 (ddd, $^2J_{P-H}$ = 4.89, $^4J_{P-H}$ = 0.75, $^2J_{H-H}$ = 7.60)		
$Cp^*(PMe_3)_2RuSi(OEt)_3$	1.69 (1.50)	h	1.42 (d, 8.28)	h	$Si(OCH_2CH_3)_3$	3.76 (q, 6.99)	2.82	7.2
					$Si(OCH_2CH_3)_3$	1.13 (t, 6.98)		

[a] Shifts are in ppm, referenced to $SiMe_4$ (δ 0.00) at 300 MHz and 30 °C in THF-d_8 unless otherwise noted. [b] Number in parentheses is $^4J_{P-H}$ in Hz. [c] Value in seconds. [d] Number in parentheses is the separation between outer lines of the filled-in doublet, $^2J_{P-H} + {}^4J_{P-H}$ in Hz. [e] Shift in ppm, referenced to 85% H_3PO_4 (δ = 0.00) at 121 MHz and 30 °C in THF-d_8, unless otherwise stated. [f] Acetone-d_6, 30 °C. [g] Not resolved. [h] Not obtained. [i] Doublet. [j] J values in hertz. T_1 values in s.

results in phosphine loss and formation of $Cp^*(PMe_3)(CO)RuNPh_2$, with no indication of products arising from insertion of CO into the Ru–NPh_2 bond. Reaction with ^{13}CO leads to the expected carbonyl band shift to lower frequency (ν(CO) = 1928 cm^{-1}, $\nu(^{13}CO)$ = 1885 cm^{-1}); the region from 1500–2000 cm^{-1} exhibits no other bands.

Attempts to prepare other ruthenium amides via metathesis with alkali metal amides have failed. Treatment of $Cp^*(PMe_3)_2RuCl$ with $LiNH(CMe_3)$ affords $Cp^*(PMe_3)Ru(\eta^2\text{-}PMe_2CH_2)$, presumably by loss of *tert*-butylamine from initially formed $[Cp^*(PMe_3)_2RuNH(CMe_3)]$ (eq 5). Reactions with other primary amide salts lead to intractable product mixtures.

$$Cp^*(PMe_3)_2RuCl \xrightarrow{Li^+NH(CMe_3)^-} Cp^*(PMe_3)Ru\!\!<\!\!\begin{matrix}P(CH_3)_2\\ CH_2\end{matrix} \quad (5)$$

The most general synthetic route to other complexes, $Cp^*(PMe_3)_2RuSH$, $Cp^*(PMe_3)_2RuCN$, $Cp^*(PMe_3)_2RuCH_2COCH_3$, $Cp^*(PMe_3)_2RuCCPh$, and $Cp^*(PMe_3)_2RuNHPh$, is via treatment of a THF solution of $Cp^*(PMe_3)_2RuOH$ with an excess of H_2S, HCN, acetone, HCCPh, or H_2NPh, respectively (eq 6). Removal of solvent and and other volatile components, extraction into

$$\underset{\mathbf{1}}{Cp^*(PMe_3)_2RuOH\cdot nH_2O} + HX \rightarrow Cp^*(PMe_3)_2RuX + (n+1)H_2O \quad (6)$$

6: X = SH
7: X = CN
8: X = CH_2COCH_3
9: X = CCPh
10: X = NHPh

hydrocarbon solvent, concentration, and crystallization at low temperature yields analytically pure samples of each of the above compounds (see Table I for spectral data). Similarly, treatment of (DPPE)MePtOMe with excess HX (X = CH_2COCH_3, CN, SH, OH) in THF is the method of choice for the preparation of (DPPE)MePtX species (vide infra).

2. Exchange Equilibria. As reported previously, addition of *N*-methylaniline to (DPPE)MePtOMe (**11**) in THF-d_8 results in the partial conversion of starting materials to methanol and (DPPE)MePtNMePh (**12**) (eq 7).[15] Measurements of the

$$\underset{\mathbf{11}}{(DPPE)MePtOMe} + HNMePh \underset{}{\overset{K_{eq}}{\rightleftharpoons}} \underset{\mathbf{12}}{(DPPE)MePtNMePh} + HOMe \quad (7)$$

concentrations of each of the components in the equilibrium by ^1H and ^{31}P NMR spectroscopy yield the equilibrium constant (K_{eq} = 0.8 ± 0.2), invariant to changes in starting conditions, moderate changes in temperature, and solvent (THF-d_8 or toluene-d_8).[16] These observations suggest that entropy contributions to the equilibrium are negligible[17] and that solvation effects are small.

The thermoneutral character of this equilibrium is quite significant. If we assume the only changes represented in the equilibrium correspond to making Pt–N and H–O bonds at the expense of Pt–O and H–N bonds, the near-unity value of K_{eq} requires the Pt–O bond in (DPPE)MePtOMe be stronger than the Pt–N bond in (DPPE)MePtNMePh by the same amount as

(15) The ramifications of the thermoneutral character observed for eq 7, in terms of homolytic and heterolytic bond strengths, has been communicated previously: Bryndza, H. E.; Fultz, W. C.; Tam, W. *Organometallics* **1985**, *4*, 939.

(16) The equilibrium constant is also independent of the reaction vessel wall material, e.g., Pyrex, silylated Pyrex, sapphire, or quartz. The authors thank Professor Herb Kaesz for suggesting *these* experiments to us.

(17) Since $\Delta G_{eq} \approx 0$ and since no measureable temperature dependence of ΔG_{eq} was noted, this shows $\Delta H_{eq} \approx \Delta S_{eq} \approx 0$.

Scheme I. L_nM-X Relative Bond Heterolysis Constants

	K_{eq}
Heterolytic Ligand Dissociation	
(1) (DPPE)MePt—OCH_3 ⇌ (DPPE)MePt$^+$ OCH_3^-	K_1
(2) (DPPE)MePt$^+$ $NCH_3(Ph)^-$ ⇌ (DPPE)MePt—NCH_3(Ph)	$1/K_2$
(3) (DPPE)MePt—OCH_3 + $NCH_3(Ph)^-$ ⇌ (DPPE)MePt—NCH_3(Ph) + OCH_3^-	K_1/K_2
(4) H^+ OCH_3^- ⇌ H—OCH_3	$1/K_a(CH_3OH)$
(5) H—NCH_3(Ph) ⇌ H^+ $NCH_3(Ph)^-$	K_a(HNMePh)
(6) H—NCH_3(Ph) + OCH_3^- ⇌ H—OCH_3 + $NCH_3(Ph)^-$	K_a(HNMePh)/$K_a(CH_3OH)$
(7) (DPPE)MePt—OCH_3 + H—NCH_3(Ph) $\overset{K}{\rightleftharpoons}$ (DPPE)MePt—NCH_3(Ph) + H—OCH_3	$\left(\frac{K_1}{K_2}\right)\left(\frac{K_a(HNMePh)}{K_a(CH_3OH)}\right)$

$K_1/K_2 \overset{K}{=} K_a(CH_3OH)/K_a$(HNMePh), since $K \overset{K}{=} 1$

the H–O bond in methanol is stronger than the H–N bond in *N*-methylaniline. Moreover, since the equilibrium constant is not solvent dependent, gas phase bond dissociation energies of 104.5 and 87.5 kcal·mol^{-1},[18] respectively, for the H-O and H-N bonds in methanol and *N*-methylaniline may be used to estimate that the Pt–O bond in (DPPE)MePtOMe is about 17 kcal·mol^{-1} stronger than the Pt–N bond in (DPPE)MePtNMePh. This functional group approach to solution phase bond dissociation energies has been exploited very effectively by Benson and others[19] in organic systems.

Another ramification of the thermoneutral character of this equilibrium concerns *heterolytic* bond dissociation constants. As illustrated in Scheme I, the equilibrium constant for eq 7 (K_{eq}) may be expressed as the product of the ratio of acid dissociation constants (K_a's) and the ratio of Pt–NMePh to Pt–OMe heterolytic dissociation constants (K_2 and K_1, respectively):

$$K_{eq} = \frac{K_1}{K_2}\frac{K_a(\text{HNMePh})}{K_a(\text{HOMe})}$$

Since K_{eq} is approximately 1, it follows that the relative extent of (DPPE)MePt–OMe and (DPPE)MePt–NMePh bond heterolysis (K_1/K_2) is equal to the relative acid dissociation constants for H–OMe and H–NMePh [K_a(HOMe)/K_a(HNMePh)]. With use of aqueous solution values of K_a for methanol and methylaniline[20] (pK_a = 16 and 25, respectively), the extent of [$NMePh^-$] dissociation from **12** in aqueous solution would be 10^9 less than [OMe^-] dissociation from **11**. While this ratio will vary as the ratio of K_a values varies in different solvents, the conclusion remains the same: the relative extent of (DPPE)MePt–X bond heterolysis parallels the relative K_a values of the H–X analogue.

The same equilibrium techniques can be used to evaluate the relative homolytic bond strengths of Pt–X bonds in a larger series: (DPPE)MePtOMe (**11**), (DPPE)MePtOH (**13**), (DPPE)MePtNMePh (**12**), (DPPE)$MePtCH_2COCH_3$ (**14**), and (DPPE)$MePtNPh_2$ (**15**) as shown in eq 8–10. Interestingly, all these reactions are also essentially thermoneutral. Other reactions of (DPPE)MePtOMe with H_2S, HCN, and $Cp(CO)_3MH$ (Cp = n^5-C_5H_5; M = Cr, Mo, W) have proven effectively irreversible;

$$\underset{\mathbf{11}}{\text{(DPPE)MePtOMe}} + \text{HOH} \rightleftharpoons \underset{\mathbf{13}}{\text{(DPPE)MePtOH}} + \text{HOMe} \quad (8)$$

$$\underset{\mathbf{11}}{\text{(DPPE)MePtOMe}} + CH_3COCH_3 \rightleftharpoons \underset{\mathbf{14}}{\text{(DPPE)}MePtCH_2COCH_3} + \text{HOMe} \quad (9)$$

$$\underset{\mathbf{11}}{\text{(DPPE)MePtOMe}} + HNPh_2 \rightleftharpoons \underset{\mathbf{15}}{\text{(DPPE)}MePtNPh_2} + \text{HOMe} \quad (10)$$

no evidence for any (DPPE)MePtOMe has been observed when (DPPE)MePtSH (**16**), (DPPE)MePtCN (**17**), and (DPPE)$MePtM(CO)_3Cp$ (**18**: M = Cr; **19**: M = Mo; **20**: M = W) were dissolved in 50/50 solutions of THF-d_8/CH_3OH (eq 11–13).

$$\underset{\mathbf{11}}{\text{(DPPE)MePtOMe}} + \text{HSH} \rightarrow \underset{\mathbf{16}}{\text{(DPPE)MePtSH}} + \text{HOMe} \quad (11)$$

$$\underset{\mathbf{11}}{\text{(DPPE)MePtOMe}} + \text{HCN} \rightarrow \underset{\mathbf{17}}{\text{(DPPE)MePtCN}} + \text{HOMe} \quad (12)$$

$$\underset{\mathbf{11}}{\text{(DPPE)MePtOMe}} + Cp(CO)_3MH \rightarrow \underset{\substack{\mathbf{18}:\ M = Cr\\ \mathbf{19}:\ M = Mo\\ \mathbf{20}:\ M = W}}{\text{(DPPE)}MePtM(CO)_3Cp} + \text{HOMe} \quad (13)$$

Attempts to extend this series to other Pt–X bonds are complicated by the high reactivity of these platinum complexes and the long times required to attain equilibrium. Fortunately, the $Cp^*(PMe_3)_2RuX$ system proved both kinetically more active in exchange equilibria and chemically more robust, providing further insights into M–X (M = Pt, Ru) homolytic bond strengths.

Reaction of $Cp^*(PMe_3)_2RuOH$ with stoichiometric amounts of diphenylamine similarly produces some $Cp^*(PMe_3)_2RuNPh_2$ and water. As in the platinum system, ^1H and ^{31}P NMR ob-

(18) (a) McMillen, D. F.; Golden, D. M. *Annu. Rev. Phys. Chem.* **1982**, *33*, 493. (b) Stull, D. R.; Westrum, E. F.; Sinke, G. C. *The Chemical Thermodynamics of Organic Compounds*; Wiley: New York, 1969. (c) Benson, S. W. *Chem. Rev.* **1969**, *69*, 279. (d) Benson, S. W. *Thermochemical Kinetics*; 2nd ed.; Wiley: New York, 1976. (e) Sanderson, R. T. *Chemical Bonds and Bond Energies*; 2nd ed.; Academic: New York, 1976.

(19) Throughout this paper we use interchangeably "L_nM-X bond strengths", "bond dissociation energies (BDEs)", and "homolytic bond strengths" to mean relative *solution phase* D(M–X) values. By using gas-phase D(H–X) values, we necessarily assume equivalent solvation of the functional groups on both sides of the equilibria and that the bonding of ancillary ligands (Cp*, phosphines, etc.) to the metal does not appreciably change. (Recent experimental measurements on the Ru–P bond dissociation enthalpies in $Cp^*(PMe_3)_2RuX$ complexes (manuscript in preparation) support such an allegation for the complexes studied here with the possible exception of the hydrides which appear to have anomalously strong Ru–P bonds. This study also bodes caution for the application of this approximation to other systems where more bulky ligands are employed.) Other studies have noted that the sublimation, dissolution, and vaporization energies needed to convert such solution data to gas-phase values make very small corrections to the relative bond strengths obtained when nongaseous reagents are involved (vide infra, ref 32). Moreover, the values and assumptions needed to correct solution phase BDEs to gas-phase numbers commonly introduce errors as large as the corrections to be made. Thus, we prefer to use the solution values obtained; we suggest the gas-phase values will be similar. The applicability of this approach is evident from the utility of the thermodynamic functional group additivity tables for organic systems in solution as well as the gas phase. See: (a) Benson, S. W. *Thermochemical Kinetics*, 2nd ed.; Wiley: New York, 1976. (b) Benson, S. W. *The Foundation of Chemical Kinetics*; Robert E. Krieger Publishing Company: Malabar, FL, 1982.

(20) While it is clear that K_a values measured in aqueous solution do not accurately reflect dissociation constants in organic solvents, such as THF, the example serves to illustrate the relative ease of ligand heterolytic dissociation in a hypothetical aqueous solvent system. The use of K_a values appropriate to different solvent systems *may* change the ratio of line 6 in Scheme I; however, any such changes, by definition, will also alter the ratio of K_1/K_2 in exactly the same way so that $K_{1solv}/K_{2solv} = K_a(HOMe)_{solv}/K_a(HNMePh)_{solv}$.

Table II

$$Cp^*(PMe_3)_2RuOH + H\text{-}X \underset{THF\text{-}d_8}{\overset{K_{eq}}{\rightleftharpoons}} Cp(PMe_3)_2Ru\text{-}X + H\text{-}OH$$

X	K_{eq}	ΔG_{eq} (kcal·mol^{-1})	rel D(Ru–X)$_{soln}$ (kcal·mol^{-1})
OH	1	0	0
CCPh	8.9	−1.3 ± 0.2	14.3
CH_2COCH_3	2.3	−0.5 ± 0.2	−20.2
NHPh	4.2	−0.9 ± 0.2	−30.1
NPh_2	0.0046	3.2 ± 0.6[a]	−37.2
SH	>8 × 10^6	<−9.4	>−18.5
CN	>8 × 10^6	<−9.4	>14.2
OCH_3	1 (calcd)	0 (calcd)	−14.6 (calcd)
H	2.12 × 10^4	−5.9 ± 0.8	−8.90

$$(DPPE)Pt\langle^{Me}_{OMe} + H\text{-}X \underset{THF\text{-}d_8}{\overset{K_{eq}}{\rightleftharpoons}} (DPPE)Pt\langle^{Me}_{X} + HOMe$$

X	K_{eq}	ΔG_{eq} (kcal·mol^{-1})	rel D(Pt–X)$_{soln}$ (kcal·mol^{-1})
OCH_3	1	0	−15.3
OH	3.2	−0.7 ± 0.2	0
NPh_2	2.5	−0.5 ± 0.2	−34.5
NMePh	0.80	0.1 ± 0.2	−32.3
CH_2COCH_3	27	−2.1 ± 0.2	−19.3
SH	>8 × 10^6	<−9.4	>−18.5
CN	>8 × 10^6	<−9.4	>14.2

$$(DPPE)Pt\langle^{Me}_{OH} + Cp^*(PMe_3)_2RuNPh_2 \underset{THF\text{-}d_8}{\overset{K_{eq}}{\rightleftharpoons}} (DPPE)Pt\langle^{Me}_{NPh_2} + Cp^*(PMe_3)_2RuOH$$

K_{eq} = 470; ΔG_{eq} = −3.6 kcal·mol^{-1}

$$Cp^*(PMe_3)_2RuSH + HSi(OEt)_3 \underset{THF\text{-}d_8}{\overset{K_{eq}}{\rightleftharpoons}} Cp^*(PMe_3)_2Ru\text{—}Si(OEt)_3 + H_2S$$

K_{eq} = 0.75; ΔG_{eq} = 0.2 ± 0.2 kcal·mol^{-1}

[a] ΔH_{eq} = 1.2 kcal·mol^{-1}.

servations show an equilibrium amount of hydroxide and amine remain (eq 14). The equilibrium constant, measured by NMR

$$Cp^*(PMe_3)_2RuOH + HNPh_2 \underset{}{\overset{K_{eq}}{\rightleftharpoons}} Cp^*(PMe_3)_2RuNPh_2 + H_2O \quad (14)$$
1 **5**

in THF-d_8 solution, is invariant to widely different starting concentrations and conditions (concentration ranges between 0.078 and 0.0065 M for $Cp^*(PMe_3)_2RuOH$ and $Cp^*(PMe_3)_2RuNPh_2$ and between 0.80 and 0.02 M for diphenylamine and water). The equilibrium constant is found to be 0.0046 (varying in a non-systematic manner between 0.0027 and 0.009), corresponding to a free energy of equilibrium of 3.2 ± 0.6 kcal·mol^{-1}.[16] The same equilibrium is established starting with $Cp^*(PMe_3)_2RuNPh_2$ and H_2O. Measurements in benzene-d_6 show the equilibrium constant is not especially solvent dependent (K_{eq} = 0.000369; ΔG = 4.7 kcal·mol^{-1}).[21]

Variable-temperature NMR measurements of the equilibrium constant for eq 14 from 20 to 55 °C in THF-d_8 show ΔH = 1.2 ± 0.1 kcal·mol^{-1} and ΔS = −6 ± 0.2 eu (Figure 1). Thus, even in this case, where a sterically uncongested hydroxide ligand is converted to a sterically demanding diphenylamido ligand on ruthenium, the entropy contribution to the equilibrium free energy amounts to only −1.8 kcal·mol^{-1} at 25 °C. These values demonstrate that the near zero free energy of equilibrium is not due to large cancelling entropy and enthalpy terms but rather to values near zero for both ΔS and ΔH. If one makes the assumptions outlined above, applying the 1.2 kcal·mol^{-1} equilibrium enthalpy correction, the Ru–O bond in $Cp^*(PMe_3)_2RuOH$ is calculated

(21) The nearly solvent independent nature of the equilibrium is further demonstrated by the fact that the [H_2O] (between 0.02 and 0.80 M), and hence the dielectric of the THF-d_8/H_2O solution, does not systematically change the measured K_{eq} for eq 14. Further evidence for the insensitivity of the equilibria measured to protic solvents comes from the study of eq 23 (vide infra) which gives results, in the absence of protic materials, which were predicted by equilibria involving those protic organic compounds.

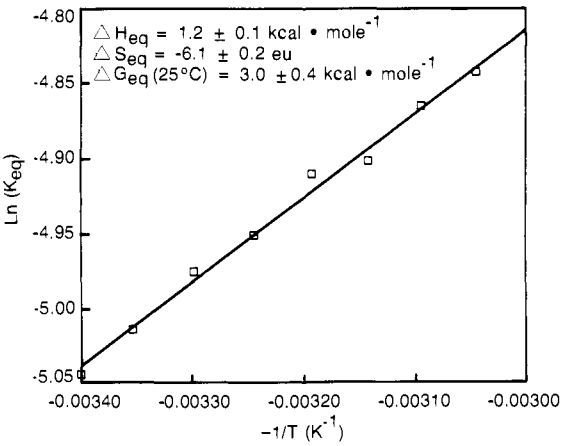

Figure 1. ln (K_{eq}) vs. $-1/T$ plot for the equilibrium $Cp^*(PMe_3)_2RuOH + HNPh_2 \rightleftharpoons Cp^*(PMe_3)_2RuNPh_2 + HOH$ between 20 and 55 °C in THF-d_8. [$Cp^*(PMe_3)_2RuX]_{total}$ = 0.05 M; [$HNPh_2$] + [H_2O] = 0.25 M. Correlation coefficient = 0.990.

to be stronger than the Ru–N bond in $Cp^*(PMe_3)_2RuNPh_2$ by about 35 kcal·mol^{-1}. Similarly, nearly thermoneutral equilibrations were found on combining $Cp^*(PMe_3)_2RuOH$ with acetone, phenylacetylene, or aniline as shown in eq 15–17.

$$Cp^*(PMe_3)_2RuOH + CH_3COCH_3 \rightleftharpoons Cp^*(PMe_3)_2RuCH_2COCH_3 + H_2O \quad (15)$$
1 **8**

$$Cp^*(PMe_3)_2RuOH + HCCPh \rightleftharpoons Cp^*(PMe_3)_2RuCCPh + H_2O \quad (16)$$
1 **9**

$$Cp^*(PMe_3)_2RuOH + H_2NPh \rightleftharpoons Cp^*(PMe_3)_2RuNHPh + H_2O \quad (17)$$
1 **10**

Reaction of $Cp^*(PMe_3)_2RuOH$ or $Cp^*(PMe_3)_2RuNPh_2$ with 4 atm of H_2 gives a mixture of $Cp^*(PMe_3)_2RuH$ (**21**) and $Cp^*(PMe_3)RuH_3$;[22] however, $Cp^*(PMe_3)_2RuH$ can be equilibrated with a large excess of H_2O (at very low H_2 pressures) as shown in eq 18. Spiking the equilibrium mixture with a small

$$Cp^*(PMe_3)_2RuH + H_2O \rightleftharpoons Cp^*(PMe_3)_2RuOH + H_2 \quad (18)$$
21 **1**

amount of pure $Cp^*(PMe_3)_2RuOH$ confirmed the presence of this constituent. Dynamic range problems limit the precision of our determination of this reaction free energy; however, the magnitude of the equilibrium constant for eq 18 does, nevertheless, establish a Ru–H bond strength relative to Ru–OH to within 4 kcal·mol^{-1}.

Irreversible reactions between $Cp^*(PMe_3)_2RuOH$ and H_2S, HCN, and $Cp(CO)_3MH$ (M = Mo, W) also take place (eq 19–21). Addition of $Cp^*(PMe_3)_2RuSH$ and $Cp^*(PMe_3)_2RuCN$

$$Cp^*(PMe_3)_2RuOH + H_2S \rightarrow Cp^*(PMe_3)_2RuSH + HOH \quad (19)$$
1 **6**

$$Cp^*(PMe_3)_2RuOH + HCN \rightarrow Cp^*(PMe_3)_2RuCN + HOH \quad (20)$$
1 **7**

$$Cp^*(PMe_3)_2RuOH + Cp(CO)_3MH \rightarrow Cp^*(PMe_3)_2RuM(CO)_3Cp \quad (21)$$
1
22: M = Mo
23: M = W

to 50/50 solutions of THF-d_8/H_2O failed to generate detectable

(22) $Cp^*Ru(PMe_3)H_3$ is in equilibrium with $Cp^*Ru(PMe_3)_2H$ at high pressure of H_2, R. Paciello and J. E. Bercaw, unpublished results.

amounts of $Cp^*(PMe_3)_2RuOH$, even at elevated temperatures. Addition of water to THF-d_8 solutions of $Cp^*(PMe_3)_2RuM(CO)_3Cp$ resulted in the formation of $Cp^*(PMe_3)_2RuH$ and products derived from the decomposition of $[CpM(CO)_3]$.

While addition of water to $Cp^*(PMe_3)_2RuSH$ failed to generate detectable amounts of the hydroxide complex **1**, addition of $HSi(OEt)_3$ establishes the equilibrium shown in eq 22. The

$$\underset{\mathbf{6}}{Cp^*(PMe_3)_2RuSH} + HSi(OEt)_3 \rightleftharpoons \underset{\mathbf{24}}{Cp^*(PMe_3)_2RuSi(OEt)_3} + H_2S \quad (22)$$

equilibrium constant of 0.75 appears to signal that second row main group substituents will be in nearly thermoneutral equilibrium with each other, although such Ru–X linkages are apparently substantially stronger than analogous bonds to comparable first row substituents, an observation consistent with the general effectiveness of sulfur and silicon compounds as catalyst poisons. An attempt to equilibrate $Cp^*(PMe_3)_2RuSH$ and Ph_2PH led instead to phosphine substitution ($Cp^*(PMe_3)(PHPh_2)RuSH + PMe_3$), contrary to what might be expected on the basis of the relative phosphine cone angles.[23]

Equilibrium measurements of the reversible reaction of $Cp^*(PMe_3)_2RuNPh_2$ with (DPPE)MePt(OH) show only a small energetic preference for $Cp^*(PMe_3)_2RuOH$ and (DPPE)$MePtNPh_2$ (eq 23). The equilibrium constant for the reaction

$$\underset{\mathbf{5}}{Cp^*(PMe_3)_2RuNPh_2} + \underset{\mathbf{13}}{(DPPE)MePtOH} \rightleftharpoons \underset{\mathbf{15}}{(DPPE)MePtNPh_2} + \underset{\mathbf{1}}{Cp^*(PMe_3)_2RuOH} \quad (23)$$

in eq 23 was found to be 470, which translates to a free energy of equilibrium of -3.6 kcal·mol^{-1}, within experimental error of the value (-3.0 ± 1.0 kcal·mol^{-1}) predicted by summing the free energies for the relevant equilibrium (eq 10–eq 8–eq 14) listed on Table II. The internally consistent nature of these equilibria further demonstrates their very small solvent dependence, since the equilibrium constants are apparently unaffected when substantial amounts of protic "co-solvents" (such as methanol, water, and diphenylamine) are present (eq 8, 10, 14), vis-à-vis absent (eq 23). Furthermore, this result suggests that the *combination* of ruthenium's preference for oxygen *and* the relief of steric crowding inherent on going from $Cp^*(PMe_3)_2RuNPh_2$ to $Cp^*(PMe_3)_2RuOH$ are small (3.6 kcal·mol^{-1}), even in the relatively congested $Cp^*(PMe_3)_2RuX$ system. The results of all such equilibrium measurements are summarized in Table II.

3. Thermolysis of $Cp^*(PMe_3)_2RuNPh_2$. Current estimates of Ru–C bond strengths of 35–45 kcal/mol,[3] combined with the series of relative bond strengths shown in Table II, indicate that the $Cp^*(PMe_3)_2Ru-NPh_2$ bond dissociation energy should fall in the range 15–25 kcal·mol^{-1}, thus suggesting that $Ru-NPh_2$ bond homolysis should occur at kinetically significant rates at easily attainable temperatures. The following observations show the Ru–N bond strength in $Cp^*(PMe_3)_2RuNPh_2$ is greater than 17 kcal·mol^{-1} and *suggest* it may be weaker than 23 kcal·mol^{-1} (although the evidence for the latter is not conclusive):

(i) Thermolysis of $Cp^*(PMe_3)_2RuNPh_2$ does indeed occur readily at 30–80 °C in benzene-d_6, accompanied by generation of tetraphenylhydrazine and its C–N bonded isomeric dimers (eq 24). Loss of **5** is between first and second order (Figure 2) as

$$\underset{\mathbf{5}}{Cp^*(PMe_3)_2RuNPh_2} \xrightarrow{30\text{–}80\ ^\circ C} N_2Ph_4\ (+\ \text{isomers}) + \ldots \quad (24)$$

might be expected from a mechanism such as that outlined in eq 25. The moderately slow rate of decomposition of **5** under these

$$\underset{\mathbf{5}}{Cp^*(PMe_3)_2RuNPh_2} \underset{k_{-1}}{\overset{k_1}{\rightleftharpoons}} \{Cp^*(PMe_3)_2Ru^{\bullet}\ {}^{\bullet}NPh_2\} \xrightarrow{k_2} N_2Ph_4 \quad (25)$$

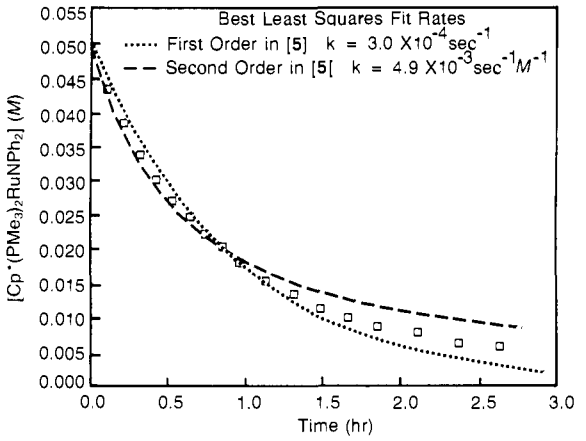

Figure 2. Thermolysis of $Cp^*(PMe_3)_2RuNPh_2$ (**5**) at 80 °C in C_6D_6 in the absence of 9,10-dihydroanthracene. Data (□) plotted as concentration (M) against time (h) with best least-squares fits of first and second order mechanisms as determined by iterative version of HAVECHEM software; see ref 46. Initial $[Cp^*(PMe_3)_2RuNPh_2]_0 = 0.051$ M. The reaction is apparently between first and second order under these conditions, with the first order line seemingly more appropriate at early times (high [**5**]) and the second order fit perhaps describing the data better when [**5**] is low.

conditions requires the Ru–N bond strength be at least 17 kcal·mol^{-1}.[24]

(ii) Thermolysis of **5** in the presence of the good hydrogen atom donor 9,10-dihydroanthracene (DHA) at 65 °C in benzene-d_6 results in clean conversion of $Cp^*(PMe_3)_2RuNPh_2$ to $Cp^*(PMe_3)_2RuH$, diphenylamine, and anthracene (eq 26) in a process which is first order in **5** (Figure 3) and first order in DHA over

$$\underset{\mathbf{5}}{Cp^*(PMe_3)_2RuNPh_2} + C_{14}H_{12} \rightarrow \underset{\mathbf{21}}{Cp^*(PMe_3)_2RuH} + HNPh_2 + C_{14}H_{10} \quad (26)$$

the range [DHA] = 0.00–1.09 M (Figure 4).[25] These observations are consistent with pre-equilibrium bond homolysis followed by competition between cage recombination[26] and hydrogen atom abstraction,[27] as shown in eq 27.

(23) Tolman, C. A. *Chem. Rev.* **1977**, *77*, 313.

(24) Since the rate of aminyl radical dimerization under these conditions is known to be 10^8–10^9 s^{-1}·M^{-1} (ref 26) and the maximum rate of radical/radical recombination can be estimated as 10^9 s^{-1}·M^{-1} from the fastest radical–radical combination rates known for diphenylaminyl radicals (ref 26), straightforward steady-state approximations indicate the rate of bond homolysis must be slower than 10^2 s^{-1}. Assuming a preexponential factor of 10^{12} (as found for diphenylaminyl radical dimerizations in benzene at 60 °C; ref 26), this corresponds to a $Ru-NPh_2$ BDE of 17 kcal/mol.

(25) Since no evidence of "saturation kinetics" (i.e., a regime in which the rate becomes less than first order in [DHA]) is observed during thermolysis at 65 °C, even in the presence of 1.09 M dihydroanthracene, the reaction mechanism represented by eq 27 is brought into question. It is well established that diphenylaminyl radicals abstract hydrogen atoms from dihydroanthracene rather inefficiently ($k_{H\ abstraction} = 10$ s^{-1}·M^{-1} at 63 °C, 2 M in benzene).[27] Therefore, the failure to observe saturation kinetics under these conditions was not entirely unexpected, given the 10^6 ratio of radical dimerization[26] to hydrogen abstraction[27] rates. Indeed, if eq 27 does accurately depict the mechanism, the observed pseudo-first-order rate constant of 3×10^{-3} s^{-1} (65 °C, [DHA] = 1.09 M) indicates that the DHA radical trapping efficiency is well below 10% of the free diphenylaminyl radicals present, the remainder being much more efficiently trapped by free {$Cp^*(PMe_3)_2Ru^{\bullet}$} to regenerate **5**.

(26) Rates for diphenylaminyl radical dimerizations have been measured in benzene from 20 to 80 °C. At 65 °C the self-dimerization rate is 10^8–10^9 s^{-1}·M^{-1} as found in the following: (a) Shida, T.; Kira, A. *J. Phys. Chem.* **1969**, *73*, 4315. (b) Welzel, P. *Chem. Ber.* **1970**, *103*, 1318. (c) Welzel, P. *Chem. Ber.* **1971**, *104*, 808. (d) Marshall, J. H. *J. Phys. Chem.* **1974**, *78*, 2225. (e) Welzel, P.; Gunther, L.; Eckhardt, G. *Chem. Ber.* **1974**, *107*, 3624. (f) Welzel, P.; Muther, I.; Volk, H. *Tetrahedron Lett.* **1977**, 745. Reports of pre-exponential factors for the N–N bond homolysis in tetraphenyl hydrazine range from log (A) = 10.4 to log (A) = 12.2 as found in ref 26a, 26d, and 26g: Cain, C. K.; Wielogle, F. Y. *J. Am. Chem. Soc.* **1940**, *62*, 1163. (h) Franzen, V. *Liebigs Ann. Chem.* **1957**, *604*, 251. (i) Zhivechkova, L. A.; Tanaseichuk, B. S.; Ermishov, A. Yu. *Zh. Org. Khim.* **1971**, *7*, 2379. (j) Tanaseichuk, B. S.; Zhivechkova, L. A.; Ermishov, A. Yu. *Zh. Org. Khim.* **1972**, *8*, 758.

$$\underset{\mathbf{5}}{Cp^*(PMe_3)_2RuNPh_2} \underset{k_{-1}}{\overset{k_1}{\rightleftharpoons}} \{Cp^*(PMe_3)_2Ru^{\bullet}\ {}^{\bullet}NPh_2\} \underset{k_{esc}}{\overset{k_{recomb}}{\rightleftharpoons}}$$

$$\{Cp^*(PMe_3)_2Ru^{\bullet}\} + \{NPh_2^{\bullet}\} \xrightarrow{k_2[DHA]} \underset{\mathbf{21}}{Cp^*(PMe_3)_2RuH} + NHPh_2 + C_{14}H_{10} \quad (27)$$

(iii) Addition of 4 equiv of free PMe_3 to a solution of $Cp^*(PMe_3)_2RuNPh_2$ containing 0.8 M DHA slightly *accelerated*, rather than slowed, the rate of reaction 26. This result suggests mechanisms involving prior phosphine dissociation from **5** are probably not involved in formation of $Cp^*(PMe_3)_2RuH$. Moreover, ^{31}P CIDNP enhanced emission signals are observed during these experiments, indicating at least some component of radical pathways. No further evidence of radical intermediates has been obtained; thermolyses conducted in ESR probes failed to reveal any detectable concentrations of paramagnetic species.[28]

Thus, failure to efficiently trap or unambiguously detect and quantify the radicals proposed in eq 25 and 27 has thwarted our attempts to confidently place an upper limit on the Ru–N bond strength for $Cp^*(PMe_3)_2RuNPh_2$. If bond homolysis is a primary step as shown in reaction 27, the pseudo-first-order rate constant of 3×10^{-3} s^{-1} for trapping less than 10% of the diphenylaminyl radicals produced when **5** is thermolyzed in the presence of 1.09 M DHA indicates a k_1 larger than 10^{-2} s^{-1}, which, in turn, places an upper limit of 23 kcal·mol^{-1} for the Ru–N bond strength for **5**.[29] Whereas this estimate does appear reasonable in view of the modest stability of **5**, even in the absence of DHA (i.e., eq 24), it should be reemphasized that the possibility that DHA reacts principally via an associative or pre-equilibrium dissociative (i.e., non-radical) pathway cannot be excluded by our data.[30] Thus, *no definite conclusions regarding the absolute magnitudes of Ru–X BDEs may be reached on the basis of the kinetics of the thermolyses of* $Cp^*(PMe_3)_2RuNPh_2$. These thermolysis experiments do place a *lower limit* on the Ru–N BDE for $Cp^*(PMe_3)_2RuNPh_2$, and hence, lower limits on all of the $Cp^*(PMe_3)_2Ru$-X complexes listed in Table II.

Discussion

The nearly thermoneutral character of the equilibria represented by eq 28 appears to be general for a number of σ-bonded ligands. This observation naturally implies that the difference in H–X and

$$L_nM\text{–}X + H\text{–}Y \overset{K_{eq}}{\rightleftharpoons} L_nM\text{–}Y + H\text{–}X \quad (28)$$

L_nM = (DPPE)MePt, $Cp^*(PMe_3)_2Ru$

H–Y BDEs is the same as the difference in L_nM–X and L_nM–Y BDEs, assuming that the functional group approach so successfully applied to organic systems by Benson[19] is equally valid for these ruthenium and platinum systems. Alternatively, one may take the observation that $K_{eq} \approx 1$ to indicate that heterolytic dissociation of basic ligands from these metal centers ($L_nM\text{–}X \rightarrow [L_nM^+] + X^-$) parallels the K_a values of the corresponding organic acids ($H\text{–}X \rightarrow H^+ + X^-$). The very small solvent dependence of the equilibrium constants allows quantitative estimates of relative homolytic bond strengths in these L_nM–X systems from the appropriate gas phase H–X bond dissociation energies.[18] This common assumption that functional groups are solvated equivalently in different complexes has proven to be valid for both organic[31] and organometallic[32] systems.

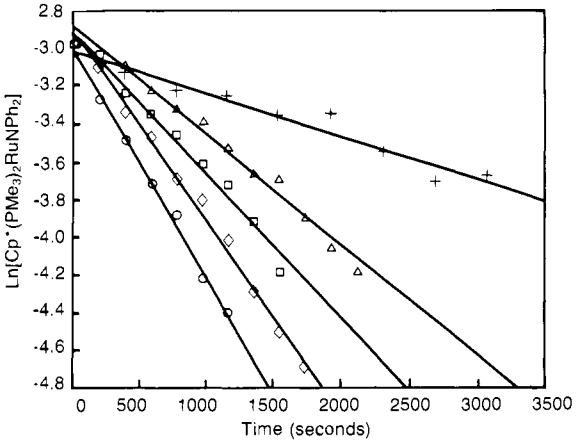

Symbol	[DHA] M	$k_{observed}$ X 10^4 (sec^{-1})	Correlation Coeff.
+	0.00	2.29 ± 0.19	0.953
△	0.42	5.81 ± 0.24	0.983
□	0.59	7.59 ± 0.39	0.990
◇	0.85	10.06 ± 0.28	0.994
○	1.09	12.33 ± 0.39	0.995

Figure 3. Thermolysis kinetics for $Cp^*(PMe_3)_2RuNPh_2$ (**5**) at 65 °C in C_6D_6 in the presence of 9,10-dihydroanthracene (DHA). Data plotted as $Ln[Cp^*(PMe_3)_2RuNPh_2]$ against time (s) for $[Cp^*(PMe_3)_2RuNPh_2]_0$ = 0.051 M; [DHA] = 0.00–1.09 M. A first order thermolysis rate for **5** in the absence of DHA was estimated from initial data although it is clear that under these conditions a first order process cannot fully explain the data in Figure 2. The initial first order rate thus obtained does fall very close to that predicted by a fit of the $k_{observed}$ vs. [DHA] data listed below the figure (and shown in Figure 4).

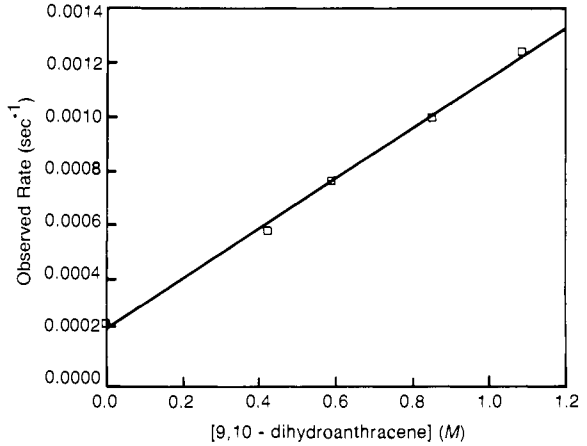

Figure 4. Order in [DHA]: thermolysis kinetics for $Cp^*(PMe_3)_2RuNPh_2$ (**5**) at 65 °C in C_6D_6 plotted as k_{obsd} (s^{-1}) vs. [DHA]. Starting conditions: [DHA] = 0.00–1.09 M; $[Cp^*(PMe_3)_2RuNPh_2]_0$ = 0.051 M; data as listed in Figure 3. Nonweighted linear least squares shows the following: $k_{obsd} = (9.27 \pm 0.20) \times 10^{-4}[DHA] + (2.14 \pm 0.01) \times 10^{-4}$ (in s^{-1}); correlation coefficient = 0.999.

(27) Rates of hydrogen atom abstraction for a variety of diarylaminyl radicals and hydrogen atom sources can be found in the following: (a) Bridger, R. F. *J. Am. Chem. Soc.* **1972**, *94*, 3124. (b) Meskina, M. Ya.; Karpukhina, G. V.; Maizus, A. K. *Izv. Akad. Nauk SSSR, Ser. Khim.* **1974**, 1755. (c) Bridger, R. F., private communication to K. U. Ingold as reported in "Landolt-Bornstein; Numerical Data and Functional Relationships in Science and Technology, New Series (editor in chief K.-H. Hellwege), Volume 13 (Radical Reaction Rates in Liquids; editor H. Fisher), subvolume c (Radicals Centered on N, S, P and other Heteroatoms; compiled by K. U. Ingold)" Springer-Verlag, Berlin 1983. The rates of hydrogen atom abstraction from 2.0 M 9,10-dihydroanthracene in benzene at 63 °C by phenyl-1-naphthylaminyl radicals is between 5 and 10 $s^{-1}\cdot M^{-1}$.

(28) As is often the case, radical lifetimes and relaxation times leading to the observation of CIDNP often preclude obtaining ESR evidence of these same radical intermediates. For a discussion of this phenomenon see: Lepley, A. R.; Closs, G. L. *Chemically Induced Magnetic Polarization*; Wiley: New York, 1973.

(29) Again (ref 24) assuming a homolysis log (A) of 12, a homolysis rate of 10^{-2} s^{-1} corresponds to a bond dissociation energy of 23 kcal·mol^{-1}.

(30) Current efforts are directed at evaluating the viability of these alternative mechanisms, including those which involve (η^6-$C_5Me_4CH_2$)-$(PMe_3)_2Ru$ and $Cp^*(PMe_3)Ru(\eta^2$-$Me_2PCH_2)$ intermediates. Some component of the loss of **5** in these thermolysis experiments can be inhibited by the presence of large concentrations of diphenylamine, suggesting a tetramethylfulvene decomposition route may account for part of the loss of **5**. The mechanism of thermolysis of the benzyl derivative, $Cp^*(PMe_3)_2RuCH_2Ph$, is also presently under investigation.

(31) Many examples are illustrated in the following: Benson, S. W. *Thermochemical Kinetics*, 2nd ed.; Wiley: New York, 1976.

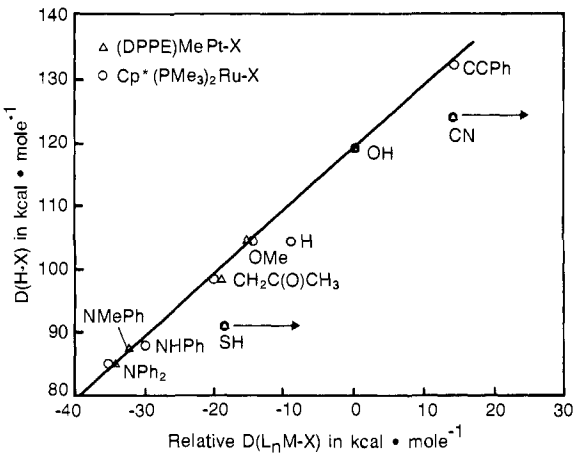

Figure 5. H–X vs. relative L_nM–X bond dissociation energies (BDEs) in kcal·mol^{-1}. Data plotted from Table II for both (DPPE)MePtX (Δ) and $Cp^*(PMe_3)_2RuX$ (O) systems with L_nM–OH arbitrarily assigned a relative BDE of 0.0 kcal·mol^{-1}. A line with an arbitrary slope of 1 has been drawn through the hydroxide "point". Data depicted for L_nM–CN and L_nM–SH are *minimum* L_nM–X bond strengths (against absolute H–X bond strengths) which, as indicated by the arrows, may be much stronger than the 9-kcal·mol^{-1} deviation detectible by our experimental methods.

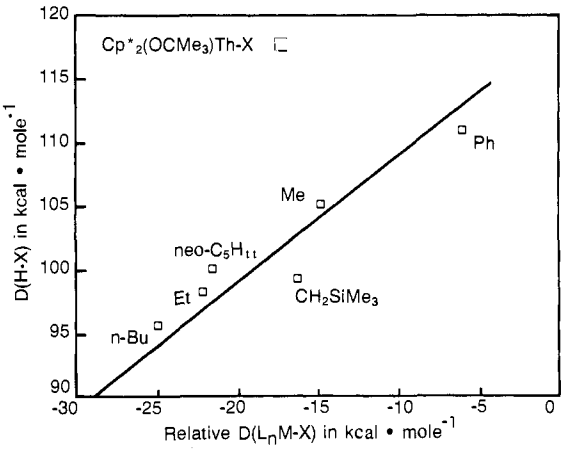

Figure 6. H–X vs. relative $Cp^*_2(OCMe_3)Th$–C bond strengths in kcal·mol^{-1}. Data taken from the solution phase values reported in ref 34 and placed on the same arbitrary scale as Figure 5 by assigning a relative Th–CH_3 bond strength of −14.9 kcal·mol^{-1}. The line is the same one depicted on Figure 5 (slope = 1.00; intercept = 119.0 kcal·mol^{-1}) with the maximum deviation of these data, noted for $Cp^*_2(OCMe_3)Th$–CH_2SiMe_3, of about 2.5 kcal·mol^{-1}. This is well within the uncertainty of the Th–X and H–X bond strengths, noting that the calorimetric methods used determine these numbers must be corrected for the heats of vaporization of gaseous products of the alcoholysis reactions; see ref 19.

An effective method of graphically illustrating the data from Table II is shown in Figure 5. For this plot of D(H–X) vs. relative $D(L_nM–X)$, the L_nM–OH bond dissociation energies for (DPPE)MePtOH and $Cp^*(PMe_3)_2RuOH$ are arbitrarily assigned a relative value of zero, and a line with a slope of 1 is drawn through this point. Two important conclusions can be drawn from the remarkably good correlation of relative H–X and L_nM–X bond strengths which is readily apparent: (i) the close linear fit for the bond dissociation energies of $\{Cp^*(PMe_3)_2Ru^\bullet\}$ and $\{(DPPE)MePt^\bullet\}$ with first row $\{X^\bullet\}$ substituents (except for the metal cyanides, vide infra) indicates that other relative L_nM–X (X = first row element) bond strengths should be predictable, even for complexes we have not yet examined, by simple extrapolation from the H–X bond strength of the organic analog; (ii) the one-to-one correlation between L_nM–X BDEs and H–X BDEs may well be generally valid for a variety of organometallic compounds, in the absence of L_nM–X multiple bonding (vide infra). That the data fit so well on the line drawn for Figure 5 is quite persuasive in this regard, since the same close correlation holds both for square planar, 16-electron, third-row (d^8) platinum complexes and for the sterically congested "three-legged-piano-stool", 18-electron, second-row (d^6) ruthenium complexes.

While examples of comparable σ-bond strength measurements for series of organometallic complexes are rare in the literature, thermochemical data on two other organometallic systems lend support to the generality of this H–X vs. relative M–X bond strength correlation. Bergman and co-workers[33] have shown that the reaction between $Cp^*(PMe_3)(H)Ir$-*cyclo*-C_6H_{11} and various alkanes does not proceed to completion to generate the corresponding alkyls and cyclohexane (eq 29), suggesting a one-to-one correspondence for Ir–C_6H_{11}, Ir–R (R = *cyclo*-C_5H_9, *neo*-C_5H_9,

$$Cp^*(PMe_3)(H)Ir\text{-}cyclo\text{-}C_6H_{11} + HR \rightleftharpoons Cp^*(PMe_3)(H)IrR + cyclo\text{-}C_6H_{12} \quad (29)$$

R =

cyclo-C_5H_9, *neo*-C_5H_9, *n*-C_5H_9, $CH_2CH(CH_3)CH(CH_3)_2$, *n*-C_5H_9, $CH_2CH(CH_3)CH(CH_3)_2$, and H–*cyclo*-C_6H_{11} H–R BDEs. Furthermore, if the (solution phase) thorium–carbon bond dissociation energies, obtained by reaction calorimetry by Bruno, Marks, and Morss,[34] are evaluated in this same manner, once again, a one-to-one correlation between $Cp^*_2(OCMe_3)Th$–R and H–R BDEs is evident (Figure 6). On the other hand, for thorium compounds with alkoxide or amide ligands, significant deviations from the one-to-one correlation are noted. For example, the $Cp^*_2(OCMe_3)Th$–OR and $Cp^*_2(OCMe_3)Th$–NR_2 BDEs are greater than would be predicted[34] for a single σ Th–OR or Rh–NR_2 bond (i.e., by comparison to the corresponding H–OR or H–NR_2 BDE). Indeed, such deviations are entirely expected, since the coordinatively unsaturated, Lewis acidic thorium center of these $Cp^*_2Th^{IV}X_2$ complexes is a powerful π-acceptor of oxygen or nitrogen lone electron pairs, increasing the Th–OR or Th–NR_2 bond order. An estimate of the thermodynamic importance of such multiple bonds can be made from the magnitude of such deviations from the 1:1 correlation expected.

Returning to the platinum and ruthenium systems, three types of compounds exhibit anomalously large L_nM–X BDEs: L_nM–CN, L_nM–SH, and $Cp^*(PMe_3)_2Ru$–H (Table II and Figure 5). The cyanide ligand is a moderate π-acceptor and, considering the extremely electron rich character of $Cp^*(PMe_3)_2Ru^{II}$, considerable ruthenium-to-cyanide back donation is anticipated, which reconciles the higher than one bond order observed. The low energy of the ν(CN) (2058 cm^{-1} for **7**; cf. ν(CN) = 2240–2260 cm^{-1} for organic nitriles[36]) is indeed indicative of substantial Ru=C=N character for $Cp^*(PMe_3)_2RuCN$ (**7**). While the platinum center in (DPPE)MePtCN is not as electron rich as the ruthenium case, similar, though reduced, M=C multiple bonding is indicated for this complex by ν(CN) of 2128 cm^{-1}.

Overlap between ruthenium or platinum σ-orbitals and the 3s/3p orbitals of the second row main group elements may be

(32) (a) Janowicz, A. H.; Periana, R. A.; Buchanan, J. M.; Kovac, C. A.; Stryker, J. M.; Wax, M. J.; Bergman, R. G. *Pure Appl. Chem.* **1984**, *56*, 13. (b) Jones, W. D.; Feher, F. J. *J. Am. Chem. Soc.* **1985**, *107*, 620. (c) Bergman, R. G. *Science* **1984**, *223*, 902. (d) Jones, W. D.; Feher, F. J. *J. Am. Chem. Soc.* **1984**, *106*, 1650. (e) Bruno, J. W.; Marks, T. J.; Morss, L. R. *J. Am. Chem. Soc.* **1983**, *105*, 6824. (f) Wax, M. J.; Stryker, J. M.; Buchanan, J. M.; Kovac, C. A.; Bergman, R. G. *J. Am. Chem. Soc.* **1984**, *106*, 1121. (g) Bryndza, H. E.; Fultz, W. C.; Tam, W. *Organometallics* **1985**, *4*, 939.

(33) Buchanan, J. M.; Stryker, J. M.; Bergman, R. G. *J. Am. Chem. Soc.* **1986**, *108*, 1537.

(34) Bruno, J. W.; Marks, T. J.; Morss, L. R. *J. Am. Chem. Soc.* **1983**, *105*, 6824.

(35) While the data for the alkoxides and amides were obtained on complexes having slightly different spectator ligand environments than the $Cp^*_2(OCMe_3)ThX$ data plotted in Figure 6, the deviations of more than 20 kcal·mol^{-1} (from the values expected based on the H–X vs. Th–X plot) are large with respect to deviations seen in Th–X bonds on changing spectator ligands. For example, in the series $Cp^*_2(OCMe_3)ThEt$, $Cp^*_2(Et)ThEt$, $Cp^*_2(Cl)ThEt$ the solution phase Th–C bond strengths range over only 4.1 kcal·mol^{-1} (76.3, 73.5, 72.2 kcal·mol^{-1}, respectively).

(36) Pasto, D. J.; Johnson, C. R. *Laboratory Text for Organic Chemistry*; Prentice-Hall: Englewood Cliffs, NJ, 1979.

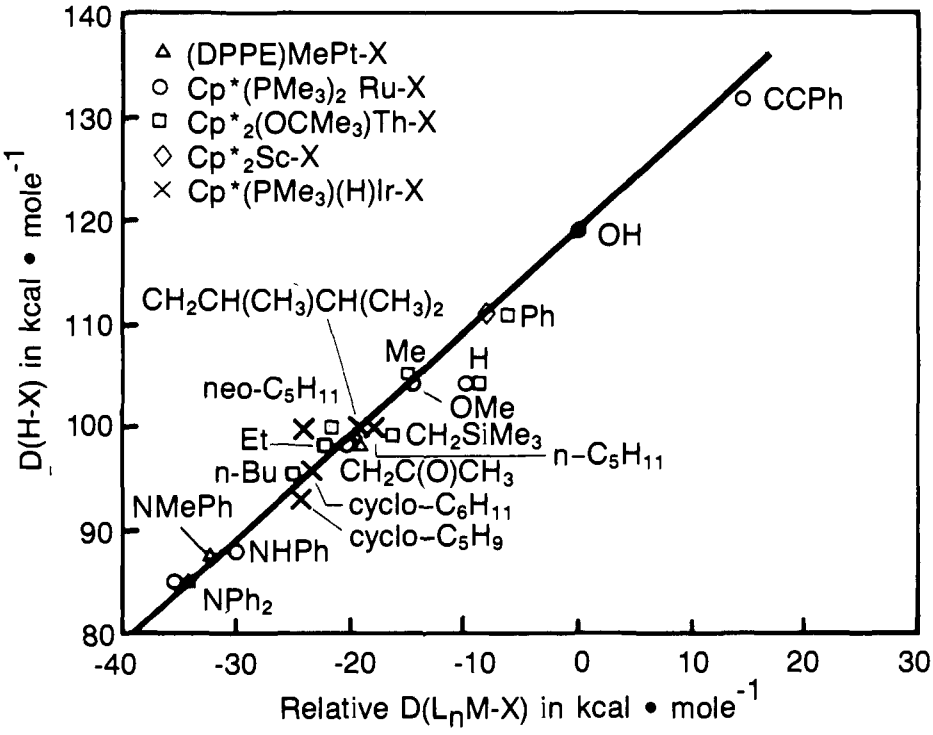

Figure 7. Cumulative plot of H–X vs. relative L_nM–X bond strengths discussed in this manuscript. Data for (DPPE)MePt–X (Δ), $Cp^*(PMe_3)_2Ru$–X (○), Cp^*_2Sc–X (◇), $Cp^*_2(OCMe_3)Th$–X (□), and $Cp^*(PMe_3)(H)Ir$–X (×) depicted for X = singly bonded first row main group substituents along with the arbitrary line (slope = 1.00; intercept = 119.0 kcal·mol^{-1}) described in Figure 5. Scale definitions for (DPPE)MePtX, $Cp^*(PMe_3)_2RuX$, and $Cp^*_2(OCMe_3)ThX$ data as described in Figures 5 and 6. To put the Sc–X data on these axes the Sc–C bond in Cp^*_2Sc–Ph has been defined as −8.1 kcal·mol^{-1}; similarly, the Ir–C bond in $Cp^*(PMe_3)(H)Ir$-*cyclo*-C_6H_{11} has been assigned an arbitrary value of −21 kcal·mol^{-1}. Good 1:1 correlation of H–X and L_nM–X bond strengths is noted.

significantly better than overlap between these metal orbitals and the 2s/2p orbitals of the first row elements. Such arguments, akin to those used to account for the preferences of "hard" and "soft" acids to bases, may be offered to explain the larger than expected L_nM–SH BDEs for **6** and **16**. In this regard, it is significant that, although $Cp^*(PMe_3)_2RuSH$ is unreactive toward a variety of first-row H–X compounds, a nearly thermoneutral equilibrium is established between $Cp^*(PMe_3)_2RuSH$, $(EtO)_3SiH$, $Cp^*(PMe_3)_2RuSi(OEt)_3$, and H_2S (eq 22). This observation suggests a second "parallel" H–X vs. relative L_nM–X bond strength correlation may hold for second row main group substituents. Because of the experimental limitations of our equilibrium measurements, we cannot quantify the energetic displacement between the L_nM–X and L_nM–Y (X = first-row substituent; Y = second-row substituent) relationships. We do, however, know the line for second-row elements must lie more than 9 kcal·mol^{-1} to the "right" of the established correlation for first-row substituents.

Although the value of the Ru–H BDE for $Cp^*(PMe_3)_2RuH$ (**21**) is rather imprecise due to the small value of the equilibrium constant for eq 18,[37] its deviation (7 kcal·mol^{-1}) from the linear correlation in Figure 5 clearly exceeds the conservative estimate of the uncertainty in the BDE of ±2 kcal·mol^{-1}. Moreover, Thompson and Bercaw[38] have found that Cp^*_2ScH reacts with benzene to establish an equilibrium mixture of Cp^*_2ScH, $Cp^*_2ScC_6H_5$, C_6H_6, and H_2, from which the thermodynamic parameters ΔH° = 6.7 (3) kcal·mol^{-1} and ΔS° = −1.5 (1) eu were obtained for eq 30. Assuming the one-to-one correlation between L_nM–X and H–X BDEs, the Sc–H BDE is 6.7 (or ca. 7.5 (4) in

$$Cp^*_2ScH + C_6H_6 \rightleftharpoons Cp^*_2ScC_6H_5 + H_2 \qquad (30)$$

the gas phase) kcal·mol^{-1} stronger than expected;[39] i.e. again, one finds that there is an increased stability associated with the L_nM–H bonds, amounting to approximately 7 kcal·mol^{-1} for the systems considered here. Even the *average* of the two Th–H BDEs in $[Cp^*_2ThH_2]_2$ (which also includes the enthalpy of the bridging interaction between the two thorium centers, which more than compensates for the loss of translational entropy due to dimerization) obtained by reaction calorimetry[34] deviates only approximately 15 kcal·mol^{-1}, again to the right of the linear correlation in Figure 6. The common assumption, based on the reported BDE difference between $(CO)_5Mn$–H and $(CO)_5Mn$–CH_3, has been that "metal–carbon" bonds in organotransition-metal compounds are approximately 25 kcal·mol^{-1} weaker than metal–hydrogen bonds.[40] Our data, and that of others cited herein, appear to indicate that (i) the difference in L_nM–H and L_nM–CH_3 BDEs is likely to be substantially smaller, and (ii) one must be cautious to correct the L_nM–R (R = alkyl, alkenyl, aryl, alkynyl, etc.) bond dissociation energy for the stability of {R•} when discussing the relative strengths of metal–carbon and metal–hydrogen bonds. As the data of Figures 5 and 6 demonstrate, metal–carbon bond strengths may be expected to vary over a range as large as 40 kcal·mol^{-1} (R = CH_2Ph to CCR′). An appropriate one-to-one comparison would be between L_nM–H and L_nM–CH_3, since the bond dissociation energies of H–H and H–CH_3 are 104 and 105 kcal·mol^{-1}, respectively.

(37) The fact that most of the dihydrogen is in the gas phase above the solution also contributes to the error in translating the Ru–H BDE for **11** to relative gas-phase values, because the enthalpy of dissolution of dihydrogen in THF, which is likely to differ substantially from the enthalpies of condensation and dissolution of the other organics used in this study, must be incorporated into the calculation. Although this quantity has not yet been measured to our knowledge, it is unlikely that it exceeds the ±2 kcal·mol^{-1} uncertainty in the measurement of the equilibrium constant for eq 18.

(38) (a) Thompson, M. E. Thesis, California Institute of Technology, 1985. (b) Thompson, M. E.; Baxter, S. M.; Bulls, A. R.; Berger, B. J.; Nolan, M. C.; Santarsiero, B. D.; Schaefer, W. P.; Bercaw, J. E. *J. Am. Chem. Soc.*, submitted for publication.

(39) Assuming a C–H BDE of 111 kcal·mol^{-1} for benzene, H–H BDE of 104 kcal·mol^{-1} and ΔH_{soln} = 0.9 kcal·mol^{-1} for H_2 in benzene.

(40) The M–CH_3 vs. M–H bond strength difference of 14 kcal·mol^{-1} quoted by Connor (*Organometallics* **1982**, *1*, 1166) has been discussed in the more recent reviews cited in ref 3 which take into account other experimental data, as well. We feel the cited value of 25 kcal·mol^{-1} more accurately reflects the perceptions of these reviews which have been widely adopted as state-of-the-art information.

Although the bond strength information presented here, as summarized for the $Cp^*(PMe_3)_2Ru-X$, (DPPE)MePt-X, $Cp^*_2(OCMe_3)Th-X$, Cp^*_2Sc-X, and $Cp^*(PMe_3)(H)Ir-X$ systems (X = singly bonded first row main group substituent) in Figure 7, is somewhat limited, we note some interesting trends. The metal–oxygen bonds examined for late metals are not, despite conventional perceptions, particularly weak. The L_nM-OH bond is stronger than L_nM-H and $L_nM-(sp^3)C$ bonds (as in the carbon-bound metal enolates **8** and **14**), but it is weaker than $L_nM-(sp)C$ bonds (as in the phenylacetylide complex **9**). Interestingly, L_nM-O bond strengths are consistently stronger than the L_nM-N bond strengths measured (for the same reasons that H–O bonds are stronger than H–N bonds), suggesting that L_nM-N bonds may be weaker than L_nM-O bonds for both early and late metal systems.[41] Substituents that weaken H–X bonds (such as phenyl substituents) will also weaken M–X bonds for the same reasons. Thus, the higher reactivity associated with (DPPE)MePt–OR (R = H, CH_3) bonds (vis-a-vis (DPPE)-(OMe)Pt–Me bonds) is kinetic rather than thermodynamic in origin.[42] Interestingly, the enhanced (greater than 9 kcal·mol^{-1}) stability of transition metal bonds to second row main group substituents, observed in both platinum and ruthenium systems, may explain the efficiency of silicon and sulfur compounds as poisons for catalysts meant for the transformation of first row main group substrates. Perhaps most importantly, the excellent correlation of H–X and relative M–X bond strengths is seen for widely disparate types of organometallic complexes and ligand environments. The same correlation appears general for first, second, and third row transition metal complexes as well as for trans-uranium elements. Both 16- and 18-electron complexes are included in Figure 7, and the trend fits data for early metal complexes as well as for late metal derivatives. Finally, the observations concerning metal–X single bonds holds for carbon, oxygen, nitrogen, and hydrogen, suggesting this correlation may be general for many types of organometallic systems.

Since the trends in M–X BDEs correlate so well with H–X BDEs, we may estimate the thermodynamics for individual steps in proposed catalytic cycles and for simple processes such as olefin or carbon monoxide insertion into L_nM-OR or L_nM-NR_2 bonds by evaluating the thermodynamics of the corresponding processes for H–OR and $H-NR_2$ (eq 31–34).[43]

$$L_nM—OH + CO \rightarrow L_nM—COOH \qquad \Delta H° \text{ } -6.8 \text{ kcal·mol}^{-1}$$

since

$$\begin{gathered} H-OH + CO \rightarrow H—COOH \\ \Delta H° = -6.8 \text{kcal·mol}^{-1} \\ L_nM—NH_2 + CO \rightarrow L_nM—CONH_2 \\ \Delta H° \text{ } -7.1 \text{ kcal·mol}^{-1} \end{gathered} \tag{31}$$

since

$$\begin{gathered} H-NH_2 + CO \rightarrow H—CONH_2 \\ \Delta H° = -7.1 \text{ kcal·mol}^{-1} \\ L_nM—OH + CH_2=CH_2 \rightarrow L_nM—CH_2CH_2OH \\ \Delta H° = -10.6 \text{ kcal·mol}^{-1} \end{gathered} \tag{32}$$

since

$$\begin{gathered} H—OH + CH_2=CH_2 \rightarrow H—CH_2CH_2OH \\ \Delta H° = -10.6 \text{ kcal·mol}^{-1} \\ L_nM—NH_2 + CH_2=CH_2 \rightarrow L_nM—CH_2CH_2NH_2 \\ \Delta H° = -19.2 \text{ kcal·mol}^{-1} \end{gathered} \tag{33}$$

since

$$\begin{gathered} H—NH_2 + CH_2=CH_2 \rightarrow H—CH_2CH_2NH_2 \\ \Delta H° = -19.2 \text{ kcal·mol}^{-1} \end{gathered} \tag{34}$$

(41) Bercaw, J. E.; Davies, D. L.; Wolczanski, P. T. *Organometallics* **1986**, *5*, 443.

(42) (a) Bryndza, H. E. *Organometallics* **1985**, *4*, 1686. (b) Bryndza, H. E. *Organometallics* **1985**, *4*, 406. (c) Bryndza, H. E.; Calabrese, J. C.; Wreford, S. S. *Organometallics* **1984**, *3*, 1603.

Our data also suggest that hydroxymethyl transition metal complexes, L_nMCH_2OH, should have approximately the same thermodynamic stability as the corresponding methoxy tautomer, L_nMOCH_3 (in the absence of oxygen-to-metal dative π-bonding, as, for example, with early transition metal systems), since according to Figures 5 and 7 there is a one-to-one trade-off of L_nM-C, H–O, H–C, and L_nM-O BDEs (eq 35). Both of these species have been proposed as key intermediates in numerous

$$L_nM-CH_2OH \overset{K_{eq}=1}{\rightleftharpoons} L_nM-OCH_3 \tag{35}$$

schemes for CO hydrogenation and alcohol homologation.[44] Hence, pathways which predominate via one of these two tautomers are likely to arise from a greater *kinetic* reactivity of that tautomer (assuming there is a facile interconversion of the two), since comparable concentrations of each should be present at equilibrium.

The relatively small difference between $M-CH_3$ and M–H bond strengths evident in some of the species discussed in this manuscript suggests that while metal alkyl hydride complexes may never become as commonplace as metal dihydrides, alkane C–H bond activation may generally produce species which are (thermodynamically) only 5–10 kcal·mol^{-1} less stable than analogous dihydrides (eq 36). While most such species may not be isolable, they are, nevertheless, energetically accessible, and therefore viable, catalytic intermediates.

$$\begin{gathered} [L_nM] + H-H \rightleftharpoons L_nMH_2 \qquad \Delta H = 0 \text{ kcal·mol}^{-1} \\ [L_nM] + H-CH_3 \rightleftharpoons L_nM(H)CH_3 \\ \Delta H = +5-10 \text{ kcal·mol}^{-1} \end{gathered} \tag{36}$$

Our data show there are surprisingly small thermodynamic consequences to steric considerations even in the rather congested $Cp^*(PMe_3)_2RuX$ derivatives though we stress that even the several kcal·mol^{-1} uncertainties inherent in our $H-X/L_nM-X$ correlation (Figures 5 and 7) can produce marked changes in product selectivities.

Summary

In summary, we note that the observed order in L_nM-X homolytic bond strengths ($L_nM-(sp)C > L_nM-O > L_nM-H > L_nM-(sp^3)C > L_nM-N$) and the insensitivity of these BDEs to steric considerations might not have been predicted prior to this work. The correlation of L_nM-X bond strengths with those of the "parent" H–X BDEs (or the stabilities of X· radicals) allows prediction of the thermodynamics accompanying many elementary processes of interest in organo-transition-metal chemistry. The thermoneutral character of equilibria graphically represented in Figure 5 also requires a correlation of the degree of L_nM-X bond heterolysis with K_a values of the corresponding organic acids, H–X. The relative extent of anion dissociation can thus be predicted within the limitations of these data, providing information about the relative importance of this step in the reaction chemistry of L_nM-X derivatives.

Experimental Section

General Considerations. All syntheses and chemical manipulations were carried out in a Vacuum Atmospheres Model HE-453 drybox equipped with either nitrogen purge or oxygen/water scrubbing recirculation "Dri-Train" or by high vacuum and Schlenk techniques. Hydrogen, nitrogen, and argon were purified by passing the streams through MnO on vermiculite followed by activated 4 Å sieves.[45] Benzene, pentane, THF, diethyl ether, and toluene were purified by distillation from

(43) Standard state used: 298.15 K, 0.1 mPa, $HCO_2H(g)$, $H_2O(g)$, CO(g), $HCONH_2(g)$, $NH_3(g)$, $CH_3CH_2OH(g)$8 $C_2H_4(g)$, $CH_3CH_2NH_2(g)$. $S°$ values unavailable for $CH_3CH_2NH_2$. Values obtained from *Journal of Physical and Chemical Reference Data*, **1982**, *11*, supplement 2.

(44) (a) Collman, J. P.; Hegedus, L. S. *Principles and Applications of Organotransition Metal Chemistry*; University Science Books: Mill Valley CA, 1980. (b) Parshall, G. W. *Homogeneous Catalysis*; Wiley: New York, 1980.

(45) Brown, T. L.; Dickerhoff, D. W.; Bafus, D. A.; Morgan, G. L. *Rev. Sci. Instrum.* **1962**, *33*, 491.

purple sodium/benzophenone ketyl solutions under argon or by vacuum transfer from the same drying and degassing medium or from "titanocene".[46] Benzene, toluene, and pentane required the addition of tetraglyme (Aldrich) to effect dissolution of the sodium. Methylene chloride was degassed by sparging with argon and then distilled, under argon, from calcium hydride. Each two liters of pentane was first washed with 3 × 100 mL of mixed H_2SO_4/HNO_3 (85/15% v/v), 1 × 100 mL of distilled water, 2 × 100 mL of saturated aqueous $NaHCO_3$ solution, and 2 × 100 mL of distilled water and filtered through $MgSO_4$ before storage over activated (350 °C, 4 h) 4 Å molecular sieves. Drybox solvents were maintained over activated 4 Å molecular sieves. Distilled water was degassed by 5 freeze–pump–thaw cycles on a high-vacuum line and methanol was first distilled from freshly prepared magnesium methoxide and degassed with 5 freeze–pump–thaw cycles. Deuterated solvents were purified and maintained in the same manner as the protonic isotopomers. Diphenylamine and 9,10-dihydroanthracene were recrystallized from pentane and vacuum dried. $LiNPh_2$ was prepared with *n*-butyllithium in pentane, and the resultant white precipitate was thoroughly washed with pentane and vacuum dried. Triflic acid, $HBF_4{\cdot}Et_2O$, KOH, phenylacetylene, aniline, methylaniline, and triethyoxysilane were degassed and used as supplied from Aldrich. Hydrogen, carbon monoxide, hydrogen sulfide, and ethylene (freeze–pump–thawed three times) were used as obtained from Matheson. ^{13}CO (Monsanto-Mound) was used as received. HCN was purified by vacuum transfer after degassing by freeze–pump–thaw cycles. **CAUTION: HCN is an extremely toxic, highly volatile liquid which may spontaneously polymerize when removed from the stabilizer it is supplied with. Extreme caution must be used when handling this compound and only well ventilated hood areas are appropriate for its use. Storage as a solid below −20 °C in an efficiently vented freezer is recommended.**

IR spectra were recorded in 0.1 mm path length KBr solution cells on a Varian Model 983G optical null spectrophotometer or in Nujol mulls on KBr plates on a Beckman IR 4230 spectrophotometer. Routine ^1H and ^{31}P spectra for characterization were obtained in benzene-d_6, THF-d_8, or acetone-d_6, with Me_4Si or H_3PO_4 as standard references, on Jeol Model FX-90Q or Jeol GX-400 spectrometers. Physical NMR measurements were made with Wilmad No. 507-TR screw-capped NMR tubes in either GE Model NT-300, NT-360, or QE-300 NMR spectrometers operating in pulsed–FT mode at 300.06, 360.80, and 300.01 MHz proton frequencies, respectively. T_1s data were acquired with Nicolet (GE) spin-inversion/recovery pulse sequences and data analysis software. For equilibrations involving hydrogen a 16-bit external digitizer was used to extend maximum dynamic range. Nuclear Overhauser enhancement (NOE) differences in ^{31}P nuclei were determined to be insignificant by integration of known-concentration solutions. Variable-temperature measurements were conducted in NMR probes calibrated with a chromel–alumel thermocouple which was, in turn, calibrated with water at 0 and 100 °C. Equilibria were evaluated by acquiring NMR spectra with use of 90° pulse lengths and at least five T_1 delay periods between pulses. Equilibrium constants were calculated by direct integration of multiple NMR spectra acquired over a period of, generally, days to weeks. A fit of the approach to equilibrium was calculated through the use of GIT software based on HAVECHEM programs.[47] Physical mass determinations were made with a Mettler Model AE160 balance calibrated with external weights and operated in a drybox. Solution concentrations were determined by standard volumetric dilution techniques or sometimes by solvent height determinations in Wilmad 507-TR screw-capped NMR tubes which were calibrated by Hamilton microliter syringes. A least-squares fit of these data shows volume (μL) = height (mm) × 14.00 + 5.55, which could be used directly to determine sample volumes. Addition of liquid components to equilibrium systems was generally measured by weight. Occasionally volume measurements were used (Hamilton μL syringe) instead.

Satisfactory elemental analysis on complexes reported were obtained from the Dornis and Kolbe Microanalytical Laboratory, the California Institute of Technology analytical service, Galbraith Microanalytical Laboratories, or Micro-Analysis Inc. Solution molecular weights were obtained by isothermal distillation with use of the Singer method.[48]

$Cp^*(PMe_3)_2RuCl$ and $Cp^*(PMe_3)_2RuR$ (**2**, R = CH_3; **3**, R = $CH_2Si(CH_3)_3$; **21**, R = H) were prepared as previously reported.[11c] (DPPE)MePtOMe (**11**)[11a] and (DPPE)MePtX (**14**, X = CH_2COCH_3; **16**, M = SH)[11b] were prepared as reported elsewhere while (DPPE)MePtX (**13**, X = OH; **17**, X = CN) were prepared as described below to give materials identical with those previously reported. The synthesis, reaction chemistry, and structural features of $(DPPE)MePtM(CO)_3Cp$ (**18**, M = Cr; **19**, M = Mo; **20**, M = W) (and other Pt–M heterobimetallic dimers) will be reported separately.[49]

Preparation of $Cp^*(PMe_3)_2RuOH$ (1). To a solution of $Cp^*(PMe_3)_2RuCH_3$ (2 g, 5 mmol) in 20 mL of Et_2O at −40 °C was added 1 equiv of CF_3SO_3H (440 μL, 5 mmol). The solution was allowed to warm to room temperature and stir for 3 h. The solution turned orange on warming and a light colored precipitate formed. A mixture of ca. 1.5 equiv of KOH (400 mg, 7.1 mmol), ca. 3 mL of H_2O (enough to completely dissolve the KOH), and 15 mL of THF was prepared and added to the cation solution at −40 °C. The combined solutions were warmed to room temperature and stirred for 3 h. All solids dissolved to yield a red-orange solution. Volatiles were removed under vacuum, and the residue was thoroughly dried. Extraction with ca. 50 mL of benzene, filtration, and freeze-drying yielded a yellow powder consisting of $Cp^*(PMe_3)_2RuOH{\cdot}nH_2O$. This extraction and freeze-drying cycle was repeated while monitoring for the appearance of the ^1H NMR peak at −5.57 ppm (in THF-d_8), which is broadened by H_2O. The resultant powder was extracted with ca. 50 mL of pentane, and the solution was filtered, reduced to ca. 10 mL, and cooled to −40 °C. Orange-red cubic crystals of anhydrous $Cp^*(PMe_3)_2RuOH$ were isolated on a cold frit and vacuum dried, 960 mg, 47.8%. The residue from the pentane extraction was recrystallized from THF to yield hydrated product, $Cp^*(PMe_3)_2RuOH{\cdot}nH_2O$, 633 mg. Combined yield 1.593 g, ca. 80%. IR (CH_2Cl_2) 3687 cm^{-1} (w). Anal. Calcd for $C_{16}H_{34}P_2ORu$: C, 47.40; H, 8.28. Found: C, 47.47; H, 8.40. Molecular weight calcd 405, found 389.

Preparation of $[Cp^*(PMe_3)_2Ru(H)Me]BF_4$ (4). To a solution of $Cp^*(PMe_3)_2RuCH_3$ (150 mg, 0.4 mmol) in 5 mL of Et_2O at −78 °C was added ca. 1 equiv of $HBF_4{\cdot}Et_2O$ (70 μL). The solution was warmed to room temperature and stirred for 15 min. A precipitate formed on warming and was isolated and washed one time with Et_2O, yielding an analytically pure white powder. Yield 123 mg, 67%. IR (Nujol) 2115 cm^{-1} (m). Anal. Calcd for $C_{17}H_{37}BF_4P_2Ru$: C, 41.56; H, 7.59. Found: C, 40.92; H, 7.45.

Preparation of $Cp^*(PMe_3)_2RuNPh_2$ (5). Twenty milliliters of THF were added at −78 °C to a mixture of $Cp^*(PMe_3)_2RuCl$ (1.5 g, 3.5 mmol) and $LiNPh_2$ (930 mg, 5.3 mmol). The solution was warmed to room temperature and stirred for 12 h. Volatiles were removed under vacuum, and the residue was thoroughly dried. Extraction with ca. 30 mL of benzene, filtration, and removal of volatiles yielded a yellow orange powder. This powder was slurried in ca. 20 mL of Et_2O, isolated on a cold frit, and washed three times with Et_2O. The resultant orange powder was recrystallized from THF. Yield 1.616 g, 82%. Anal. Calcd for $C_{28}H_{43}NP_2Ru$: C, 60.43; H, 7.73; N, 2.52. Found: C, 60.31; H, 7.83; N, 2.51.

Preparation of $Cp^*(PMe_3)_2RuSH$ (6). To a solution of $Cp^*(PMe_3)_2RuOH$ (200 mg, 0.5 mmol) in 10 mL of Et_2O at −78 °C was introduced 1 atm of H_2S. The solution was warmed to room temperature and stirred for 15 min. A white precipitate formed on warming and dissolved on continued stirring. Volatiles were removed under vacuum, and the residue was extracted with ca. 10 mL of petroleum ether. The solution was filtered, reduced to ca. 3 mL, and slowly cooled to −78 °C. The resultant yellow crystals were isolated on a cold frit and dried under vacuum. Yield 145 mg, 69.4%. IR (Nujol) 2508 cm^{-1} (w). Anal. Calcd for $C_{16}H_{34}SP_2Ru$: C, 45.59; H, 8.13. Found: C, 45.93; H, 7.92.

Preparation of $Cp^*(PMe_3)_2RuCN$ (7). To a solution of $Cp^*(PMe_3)_2OH$ (100 mg, 0.25 mmol) in 5 mL of THF was added 30 μL of liquid HCN in a cold syringe. The solution lightened immediately and was stirred for 15 min before the volatiles were removed under vacuum into a trap containing an aqueous bleach solution which was subsequently thawed in a well-ventilated hood. The resulting oil was redissolved in 0.5 mL of THF, and pentane was added until the mixture became cloudy (ca. 5 mL). The solution was cooled to −40 °C, and the resulting crystals were collected on a cold frit and dried under vacuum. Yield 57 mg, 56%. IR (THF) 2058 cm^{-1} (s). Anal. Calcd for $C_{17}H_{33}NP_2Ru$: C, 49.26; H, 8.03. Found: C, 49.58; H, 8.05.

Preparation of $Cp^*(PMe_3)_2RuCH_2C(O)CH_3$ (8). To a solution of $Cp^*(PMe_3)_2RuOH$ (228 mg, 0.56 mmol) in 10 mL of THF was added 1.5 mL of acetone (20 mmol) at −40 °C. The solution was warmed to room temperature and stirred for 12 h. Volatiles were removed under vacuum, and the resultant residue was extracted thoroughly with petroleum ether. The solution was filtered, reduced to ca. 10 mL, and cooled to −78 °C. The orange yellow crystals were isolated on a cold frit and dried under vacuum. The supernatant was reduced to yield a second crop. Combined yield 191 mg, 76%. IR (CH_2Cl_2) 1601 cm^{-1} (s), 1771

(46) Marvich, R. H.; Brintzinger, H. H. *J. Am. Chem. Soc.* **1972**, *94*, 2046.

(47) An iterative least-squares version of HAVECHEM (as reported in: Stabler, R. N.; Chesnick, J. *Int. J. Chem. Kinet.* **1978**, *10*, 461) has been developed at DuPont by Dr. F. J. Weigert.

(48) (a) Singer, J. A. *Justus Liebigs Ann. Chem.* **1930**, *478*, 246. (b) Clark, E. P. *Ind. Eng. Chem., Anal. Ed.* **1941**, *13*, 820.

(49) Bryndza, H. E.; Janowicz, A. H.; Fultz, W. C., manuscript in preparation.

cm^{-1} (m). Anal. Calcd for $C_{19}H_{38}OP_2Ru$: C, 51.22; H, 8.60. Found: C, 51.34; H, 8.58.

Preparation of $Cp^*(PMe_3)_2RuCCPh$ (9). To a solution of $Cp^*(PMe_3)_2RuOH$ (423 mg, 1.04 mmol) in 10 mL of THF was added HCCPh (1.14 mL, 10.4 mmol). The solution was stirred at room temperature for 12 h. Volatiles were removed under vacuum, and the residue was slurried in petroleum ether (10 mL) and THF (ca. 2 mL, enough to dissolve the complex). The solution was filtered, reduced to ca. 6 mL, and slowly cooled to −78 °C. The supernatant was removed from the resultant orange crystals and concentrated to yield a second crop. Combined yield 387 mg, 75%. IR (Nujol) 2060 cm^{-1} (s), 2000 cm^{-1} (w). Anal. Calcd for $C_{24}H_{38}P_2Ru$: C, 58.88; H, 7.82. Found: C, 58.62; H, 7.56.

Preparation of $Cp^*(PMe_3)_2RuNHPh$ (10). To a solution of $Cp^*(PMe_3)_2RuOH$ (473 mg, 1.17 mmol) in 10 mL of THF was added H_2NPh (1.06 mL, 11.6 mmol). The solution was stirred at room temperature for 12 h. Volatiles were removed under vacuum, and the resultant solid was slurried in petroleum ether (10 mL) and THF (ca. 2 mL, enough to dissolve the complex). The solution was filtered, reduced in volume to ca. 6 mL, and slowly cooled to −78 °C. The supernatant was removed from the crystals and reduced to yield a second crop. Combined yield 356 mg, 64%. IR (Nujol) 3320 cm^{-1} (w). Anal. Calcd for $C_{22}H_{39}NP_2Ru$: C, 54.98; H, 8.18; N, 2.91. Found: C, 55.28; H, 8.00; N, 2.78.

Preparation of $Cp^*(PMe_3)_2Ru(\eta^2\text{-}PMe_2CH_2)$. Twenty milliliters of THF were added to a mixture of $Cp^*(PMe_3)_2RuCl$ (1.0 g, 2.4 mmol) and 2 equiv of LiNH(*t*-Bu) (412 mg, 5.0 mmol) at −78 °C. The solution was warmed to room temperature and stirred for 12 h. Volatiles were removed under vacuum, and the residue was thoroughly dried. Extraction with petroleum ether (ca. 50 mL), filtration, and removal of volatiles under vacuum yielded a red oil. This oil was frozen then broken up by vigorous stirring under petroleum ether at −78 °C to yield an analytically pure yellow powder which was isolated and dried on a cold frit. Yield 580 mg, 63%. Anal. Calcd for $C_{16}H_{32}P_2Ru$: C, 49.61; H, 8.32. Found: C, 49.85; H, 8.27.

Preparation of $Cp^*(PMe_3)_2RuM(CO)_3Cp$ (22, M = Mo; 23, M = W). Both complexes were prepared by the same method which follows. To a solution of 100 mg (0.25 mmol) of $Cp^*(PMe_3)_2RuOH$ in 5 mL of THF was added $Cp(CO)_3MoH$ (59 mg, 0.25 mmol). The resulting solution was stirred for 3 h and filtered through a medium frit. The filtrate was evaporated to dryness under vacuum, and the resulting oil was redissolved in minimal THF (ca. 1 mL). This solution was layered with 10 mL of pentane and carefully set in a drybox freezer to mix over the course of 72 h. The resulting crystals were filtered and vacuum dried to give 130 mg (0.21 mmol, 83%) of the heterobimetallic product. Anal. Calcd for $C_{24}H_{38}O_3P_2MoRu$: C, 46.23; H, 6.14. Found: C, 46.03; H, 5.84. Similarly, using 83 mg (0.25 mmol) of $Cp(CO)_3WH$ led to isolation of 151 mg (0.21 mmol, 83%) of product. Anal. Calcd for $C_{24}H_{38}O_3P_2RuW$: C, 39.96; H, 5.31. Found: C, 39.83; H, 5.21.

Preparation of $Cp^*(PMe_3)_2RuSi(OEt)_3$ (24). In a 5-mm screw-capped NMR tube 17 mg (0.040 mmol) of $Cp^*(PMe_3)_2RuSH$ were dissolved in 600 μL of THF-d_8 and treated with 26 mg (0.32 mmol, 8 equiv) of $HSi(OEt)_3$. The tube was sealed and gently warmed (45 °C) for 5 days during which time complete conversion of the starting material was noted. Addition of pentane (2 mL) to the tube followed by cooling for 48 h at −40 °C gave 9 mg (0.016 mmol, 41%) of the desired silane. No evidence for the formation of any ruthenium(IV) $Cp^*(PMe_3)Ru(H)(Si(OEt)_3)_2$ was noted at any time during the thermolysis.

Preparation of (DPPE)MePtX (12, NMePh; 15, X = NPh_2). Both complexes were prepared by the same method. A total of 1.00 g (1.55 mmol) of (DPPE)MePtCl was slurried in 150 mL of THF and treated with 1.00 equiv (114 mg) of LiNMePh. The mixture was stirred for 4 h at room temperature during which time the off-white slurry became a homogeneous yellow solution. Solvent removal under vacuum followed by extraction of the resulting solid with 3 × 50 mL of benzene gave a yellow solution which was filtered and concentrated, under vacuum, to a total volume of ca 40 mL. Pentane (80 mL) was added and the resulting yellow solid was collected in a frit and vacuum dried to yield 855 mg (1.20 mmol, 77%) of **12**. NMR: ^1H(THF-d_8/THF-d_7) δ 7.80 (m, 4 H), 7.69 (m, 4 H), 7.48 (m, 6 H), 7.30 (m, 6 H), 6.69 (t, J = 8 Hz, 2 H), 6.48 (d, J = 8 Hz, 2 H), 5.91 (t, J = 7 Hz, 1 H), 5.37 (d, J = 3.4 Hz, J_{Pt} = 34 Hz, 3 H), 2.3 (m, 4 H), 0.52 (dd, J = 4.7, 7.8 Hz, J_{Pt} = 64 Hz, 3 H) ppm. ^{31}P(THF-d_8/H_3PO_4 external) δ 38.34 (d, J_{PP} = 4.4 Hz, J_{Pt} = 1685 Hz), 39.53 (d, J_{PP} = 4.4 Hz, J_{Pt} = 3072 Hz) ppm. ^{13}C(THF-d_8/Me_4Si external) δ 2.27 (dd, J = 6.1, 99.0 Hz, J_{Pt} = 574 Hz), 26.9 (dd, J = 9.7, 32.7 Hz, J_{Pt} = 49 Hz), 29.7 (dd, J = 15.8, 38.1 Hz, J_{Pt} = 30 Hz), 39.4 (s, J_{Pt} = 37 Hz), aromatic at 133 (complex), 130.7 (dd, J = 1.8, 53.9 Hz), 128.7 (dd, J = 9.9, 19.6 Hz), 127.6, 131.8 (complex), 159.1 (d, J = 1.7 Hz, J_{Pt} = 24 Hz) ppm. Anal. Calcd for $C_{34}H_{35}NP_2Pt$: C, 57.14; H, 4.93; P, 8.67; N, 1.96. Found: C, 57.24; H, 4.86; P, 8.48; N, 2.19. By this same technique 640 mg (0.82 mmol, 53%) of **15** was isolated from the reaction of 1.00 g (1.55 mmol) of (DPPE)MePtCl with 1 equiv of $LiNPh_2$ (275 mg). NMR: ^1H(THF-d_8/THF-d_7) δ 6.3–7.8 (m, 20 H), 2.3 (m, 4 H), 0.59 (dd, J = 4.5, 7.5 Hz) ppm. ^{31}P(THF-d_8/H_3PO_4 external) δ 40.85 (d, J_{PP} = 3.2 Hz, J_{Pt} = 1688 Hz), 39.89 (d, J_{PP} = 3 Hz, J_{Pt} = 3307 Hz) ppm. Anal. Calcd for $C_{39}H_{37}NP_2Pt$: C, 60.30; H, 4.80. Found: C, 60.18; H, 4.78.

Preparation of (DPPE)MePtX (17, X = CN; 13, X = OH). A solution of 100 mg (0.16 mmol) of (DPPE)MePtOMe was dissolved in 20 mL of THF and treated with 30 μL of liquid HCN (0.78 mmol) with use of a cold syringe. The solution lightened instantly and was stirred for 30 min before the volatiles were removed, under vacuum, into a trap containing an aqueous bleach solution. The trap was subsequently thawed in a well-ventilated hood. The resulting solid was recrystallized from hot THF/pentane to yield 85 mg (0.13 mmol, 86%) of **17**. NMR parameters were identical with those reported by Bennett.[11b] IR-(CH_2Cl_2): ν(CN) = 2128 cm^{-1}. In a similar manner, (DPPE)MePtOH was prepared by adding an excess (500 mg, 28 mmol) of degassed water to a THF solution of (DPPE)MePtOMe in THF to give material identical with that reported by Bennett.[11b]

Reaction of $[Cp^*(PMe_3)_2Ru(Et_2O)]^+OTf^-$ with NaOMe. To a solution of $Cp^*(PMe_3)_2RuCH_2SiMe_3$ (250 mg, 0.53 mmol) in 10 mL of Et_2O at −78 °C was added 1 equiv of CF_3SO_3H (47 μL, 0.53 mmol). The solution was warmed to room temperature, stirred for 1 h, and cooled to −78 °C again. Na metal (1.1 equiv, 13 mg, 0.57 mmol) was added to 3 mL of MeOH; upon complete reaction, the solution was cooled to −78 °C and added to the solution of ruthenium cation. The reaction appeared instantaneous, yielding a yellow solution; the mixture was allowed to stir for 15 min. Volatiles were removed under vacuum at the lowest possible temperature, ca. 5–10 °C, and the residue was dried thoroughly and extracted with 40 mL of petroleum ether. Filtration, reduction in volume, and cooling to −78 °C afforded yellow crystals which were isolated on a cold frit. The product was identified as $Cp^*(PMe_3)_2RuH$ by comparison to an authentic sample. Yield 205 mg, 82%.

Carbonylation of $Cp^*(PMe_3)_2RuNPh_2$. A 20-mg sample of $Cp^*(PMe_3)_2RuNPh_2$ in 0.3 mL of benzene-d_6 in an NMR tube was sealed under 1 atm of CO at −196 °C and allowed to warm to room temperature. The subsequent reaction was monitored by ^1H NMR; upon apparent completion, the tube was opened under an inert atmosphere and an infrared spectrum of the contents obtained (C_6D_6 vs. C_6D_6); ν(CO) = 1928 cm^{-1}. The experiment was repeated with ^{13}CO; ν(^{13}CO) = 1885 cm^{-1} (predicted 1858 cm^{-1}), no other bands were observed to shift from 1500 to 2000 cm^{-1}.

Reaction of $Cp^*(PMe_3)_2RuSH$ with $HPPh_2$. To a 15-mg sample of $Cp^*(PMe_3)_2RuSH$ in 0.3 mL of benzene-d_6 was added ca. 5 equiv of $HPPh_2$ (30 μL), and the tube was heated at 80 °C until apparent completion of reaction (2 h). A single product was observed by ^1H and ^{31}P NMR and assigned as $Cp^*(PMe_3)(HPPh_2)RuSH$.

Equilibrium Studies. In a typical experiment 17.0 mg (0.0266 mmol) of (DPPE)MePtOMe was dissolved in approximately 600 μL of THF-d_8 in a 5 mm Wilmad No. 507 TR screw-capped NMR tube. The tube was charged with 25.3 mg (0.236 mmol) of methylaniline and 9.8 mg (0.31 mmol) of methanol before being tightly sealed. NMR spectra were acquired as previously described, and an equilibrium constant was determined after 10 days at 25.4 °C. Confirmation of this constant was obtained by fitting the time-dependent concentration data using the software described. The same equilibrium was established from (DPPE)MePtNMePh and methanol to confirm the reversible nature of the reaction and concentrations of starting materials ranging from 0.005 to 0.021 M Pt, and 0.015 to 0.95 M organics were studied. Heating the solution at 45 °C for 10 days followed by remeasuring the equilibrium constant confirmed the temperature independence of this equilibrium. Other more robust complexes were heated over a wider range. Absolute concentrations of individual reagents were determined from the quantities added and the height of solution in the NMR tube although only the ratios really mattered in the equilibrium calculations. Other equilibrium studies (as indicated on Table II) were conducted in similar fashion. Equilibration times ranged from minutes to weeks, depending on the exact equilibrium involved.

$Cp^*(PMe_3)_2RuNPh_2$ Thermolyses. In a 5 mm Wilmad No. 507 TR screw-capped NMR tube a solution of 17.5 mg (0.032 mmol, 0.052 M) of $Cp^*(PMe_3)_2RuNPh_2$ in 600 μL of C_6D_6 was heated at 80 °C. The concentration of amide was determined by integration of the ^{31}P NMR spectra acquired, which is shown in Figure 2. Another experiment conducted at 0.018 M amide concentration interestingly fit a second-order decay much better than a first-order process. A similar experiment was conducted at 30 °C ([$Cp^*(PMe_3)_2RuNPh_2$] = 0.052 M) with the same results; an initial rate constant obtained by first-order fit of the first few points was ca. 10^{-7} s^{-1}, which is very slow on the time scale of the equilibria involving this complex. Organic thermolysis products were

determined by capillary gas chromatography on a 25-m methylsilicone column in a Hewlett Packard Model 3890 gas chromatograph with use of both N,P-thermionic and flame ionization detectors. An authentic sample of tetraphenylhydrazine was thermolyzed in benzene-d_6 at 80 °C and used to confirm the identity of the products obtained.

Amide thermolysis in the presence of 9,10-dihydroanthracene was carried out in benzene-d_6 at 65 °C by the same techniques. Both amide and DHA were added to the NMR tubes and solvent was added. Concentrations were determined by sample height. Concentration vs. time data were acquired automatically with Nicolet KINET software and was analyzed with RS1 software operating on a VAX 11/780 system. Figure 3 shows the loss of amide plots obtained, while the rate dependence on dihydroanthracene is shown on Figure 4. Products were identified by spiking product solutions with authentic samples of $Cp^*(PMe_3)_2RuH$, $HNPh_2$, and anthracene. Both GC and NMR methods were used.

When trimethylphosphine was added to a solution of amide and 9,10-dihydroanthracene in benzene-d_6 ($[Cp^*(PMe_3)_2RuNPh_2] = 0.052$ M; $[PMe_3] = 0.20$ M; [9,10-DHA] = 0.80 M) thermolysis at 60 °C demonstrated the loss of amide to be faster than in the absence of phosphine. Only ca. 60% of the amide was converted to hydride in this case (the other products were not identified), and during the thermolysis ^{31}P CIDNP signals were noted.

Acknowledgment. The technical assistance of Martin A. Cushing, Jr., Joseph P. Foster, Jr., and Barry D. Johnson is gratefully acknowledged. We also appreciate the efforts of Mr. E. A. Conaway in obtaining some of the T_1s data needed for these studies. We thank Drs. David M. Golden and Gregory P. Smith of the Chemical Kinetics research group at SRI International and Professor Robert H. Grubbs at CIT for valuable discussions. This work was supported by the DuPont Company and, in part, by the National Science Foundation (Grant CHE-8303735), which is gratefully acknowledged.

A Kinetic Study of the Epoxidation of 2,3-Dimethyl-2-butene by *tert*-Butyl Hydroperoxide Catalyzed by Imidazole Ligated (*meso*-Tetraphenylporphinato)manganese(III)

P. N. Balasubramanian, Ashoke Sinha, and Thomas C. Bruice*

Contribution from the Department of Chemistry, University of California at Santa Barbara, Santa Barbara, California 93106. *Received May 12, 1986*

Abstract: A kinetic study of the epoxidation of 2,3-dimethyl-2-butene (TME) by *t*-BuOOH in the presence of (*meso*-tetraphenylporphinato)manganese(III) chloride ((TPP)$Mn^{III}Cl$) and imidazole (ImH) has been carried out (30 °C, CH_2Cl_2 solvent). The rates of decrease in [*t*-BuOOH] and increase in [epoxide] have been determined as a function of the initial concentrations of [*t*-BuOOH], [TME], [ImH], and [(TPP)$Mn^{III}Cl$]. As found previously, ImH ligation is required for the reaction of the manganese(III) porphyrin with *t*-BuOOH and thus for the epoxidation of TME. Under the condition of $[t\text{-BuOOH}]_i$, $[TME]_i$, and $[ImH]_i \gg [(TPP)Mn^{III}Cl]_i$, it is found that the rate for disappearance of *t*-BuOOH is always more than twofold greater than is the rate of epoxide formation regardless of the ratios of [*t*-BuOOH], [ImH], and [TME]. This requires that in addition to an ImH ligated higher valent manganese oxo porphyrin there is the formation of an additional intermediate species capable of transferring oxygen. This must be so, because the total concentration of (TPP)$Mn^{III}Cl$ is not sufficient to store the oxygen equivalents. Other pertinent observations are as follows: (i) Disappearance of *t*-BuOOH follows the first-order rate law in the absence of TME while in the presence of TME its disappearance follows two sequential first-order processes; (ii) formation of epoxide is always first-order; (iii) the maximum yield of epoxide is but ~60%; (iv) the % yield of epoxide increases and then decreases with increase in $[ImH]_i$; and (v) there is formation of a small percentage of di-*tert*-butyl peroxide ($(t\text{-BuO})_2$). A proposed reaction sequence which is competent in accounting for these observations is presented in Scheme I. The equilibrium constants for ligation of ImH with manganese(III) porphyrin and the rate constants for oxygen transfer from *t*-BuOOH to both (TPP)Mn^{III}(ImH)Cl and (TPP)$Mn^{III}(ImH)_2$ were determined individually while the other constants of Scheme I were obtained as the best minimal values by computer simulation of the time dependence for the disappearance of *t*-BuOOH and appearance of epoxide and $(t\text{-BuO})_2$.

The impetus to study oxygen atom transfer oxidations with iron(III) and manganese(III) porphyrins has been to gain basic chemical knowledge essential to an understanding of the mechanisms of the peroxidase and cytochrome P-450 enzymes and also to provide new synthetic approaches to such reactions as oxygen insertion into C–H bonds and selective epoxidations.[1,2] (*meso*-Tetraphenylporphinato)manganese(III) chloride ((TPP)$Mn^{III}Cl$) is a good catalyst for oxidations with iodosylbenzene and percarboxylic acids but not reactive with alkyl hydroperoxides[3] as such. Ligation by imidazoles[4] and pyridines[5] greatly enhances the reactivity of manganese(III) porphyrin salts with alkyl hydroperoxides and hypochlorite. Mansuy et al.[4c] reported that addition of imidazole increases the yield of epoxide when using cumyl hydroperoxide as an oxidant with a manganese(III) porphyrin. In quantitative studies, we have shown that exchange of Cl^- ligand for imidazole (ImH) dramatically increases the rate constants for oxygen transfer to manganese(III) porphyrin from both percarboxylic acids and alkyl hydroperoxides.[6] The former reaction involves rate-determining heterolytic O–O bond scission and the latter most likely rate-determining homolytic bond scission.

(1) (a) Morrison, M.; Schonbaum, G. R. *Annu. Rev. Biochem.* **1976**, *45*, 861. (b) Dunford, H. B.; Stillman, J. S. *Coord. Chem. Rev.* **1976**, *19*, 187. (c) Coon, M. J.; White, R. E. In *Metal Ion Activation of Dioxygen*; Spiro, T. G., Ed.; John Wiley and Sons: New York, 1980; pp 73–123. (d) Omura, T. In *Cytochrome P-450*; Sato, R., Omura, T., Eds.; Kodansha Ltd.: Tokyo, 1978; pp 138–163. (e) Ullrich, V. *J. Mol. Catal.* **1980**, *7*, 159.

(2) Gelb, M. H.; Toscano, W. A., Jr.; Sligar, S. G. *Proc. Natl. Acad. Sci. U.S.A.* **1982**, *79*, 5758.

(3) (a) Yuan, L.-C.; Bruice, T. C. *Inorg. Chem.* **1985**, *24*, 986. (b) Mansuy, D.; Bartoli, J.-F.; Momenteau, M. *Tetrahedron Lett.* **1982**, *23*, 2781. (c) Mansuy, D.; Bartoli, J.-F.; Chottard, J.-C.; Lange, M. *Angew. Chem., Int. Ed. Engl.* **1980**, *19*, 909. (d) Hill, C. L.; Smegal, J. A.; Henly, T. J. *J. Org. Chem.* **1983**, *48*, 3277.

(4) (a) Collman, J. P.; Brauman, J. I.; Meunier, B.; Hayashi, T.; Kodadek, T.; Raybuck, S. A. *J. Am. Chem. Soc.* **1985**, *107*, 2000. (b) Collman, J. P.; Brauman, J. I.; Meunier, B.; Raybuck, S. A.; Kodadek, T. *Proc. Natl. Acad. Sci. U.S.A.* **1984**, *81*, 3245. (c) Mansuy, D.; Battioni, P.; Renaud, J.-P. *J. Chem. Soc., Chem. Commun.* **1984**, 1255.

(5) (a) Guilmet, E.; Meunier, B. *Nouv. J. Chim.* **1982**, *6*, 511. (b) Meunier, B.; Guilmet, E.; Carvalho, M.-E. D.; Poilblanc, R. *J. Am. Chem. Soc.* **1984**, *106*, 6668. (c) Collman, J. P.; Kodadek, T.; Raybuck, S. A.; Meunier, B.; *Proc. Natl. Acad. Sci. U.S.A.* **1983**, *80*, 7039. (d) Guilmet, E.; Meunier, B. *J. Mol. Catal.* **1984**, *23*, 115. (e) Van der Made, A. W.; Nolte, R. J. M. *J. Mol. Catal.* **1984**, *26*, 333. (f) Razenberg, J. A. S. J.; Nolte, R. J. M.; Drenth, W. *Tetrahedron Lett.* **1984**, *25*, 789.

(6) Yuan, L.-C.; Bruice, T. C. *J. Am. Chem. Soc.* **1986**, *108*, 1643.

0002-7863/87/1509-1456$01.50/0